Distribution and isotopic signature of ligand-leachable particulate iron along the GEOTRACES GP16 East Pacific Zonal Transect

Marsay Chris M. [1, *], Lam Phoebe J. [2], Heller Maija Iris [2], Lee Jong-Mi [2], John Seth G. [1, 3]

[1] Department of Earth and Ocean Sciences, University of South Carolina, Columbia, SC 29208, USA
[2] Department of Ocean Sciences, University of California, Santa Cruz, CA 95064, USA
[3] Department of Earth Science, University of Southern California, Los Angeles, CA 90089, USA

* Corresponding author : Chris M. Marsay, email address : christopher.marsay@skio.uga.edu

Abstract :

Particles play an important role in the marine biogeochemical cycling of iron, an essential micronutrient. Particles of biogenic, lithogenic and authigenic origin can act as sources or sinks of dissolved iron and therefore influence its distribution and availability to phytoplankton. However, not all particulate Fe (pFe) is readily accessible to phytoplankton and various treatments are used to estimate the bioavailable, or labile fraction of pFe. Here we report concentration and iron stable isotope data for the "ligand-leachable" fraction of pFe, following the application of a pH 8 oxalate-EDTA leach to 0.8–51 μm-sized particles collected during the US GEOTRACES East Pacific Zonal Transect (GP16). Across the GP16 section, we identified two regions of high labile pFe concentrations and differing $\delta^{56}Fe_{labile}$. Within a hydrothermal plume originating from the East Pacific Rise, nearly all of the pFe was labile, with concentrations as high as 42 nM. Particulate $\delta^{56}Fe_{labile}$ within the hydrothermal plume averaged − 0.26 ± 0.14‰ (n = 67), which is similar to both dissolved hydrothermal plume $\delta^{56}Fe$ and the $\delta^{56}Fe$ of primary vent fluids from previous studies, suggesting that vent fluid Fe is quantitatively precipitated as labile Fe oxyhydroxides and that the chemical form of hydrothermal dissolved and particulate Fe are the same, though they are found in different size classes. Elevated pFe concentrations were also observed over the Peruvian continental shelf and extending westwards, coincident with the secondary nitrite maximum at the top of the oxygen minimum zone (OMZ). Again, most of the pFe was within the labile fraction, but the $\delta^{56}Fe_{labile}$ associated with the OMZ was lighter than in the hydrothermal plume (− 0.68 ± 0.32‰, n = 41), reflecting its origin within reducing continental margin sediments. The open ocean away from these features was characterized by labile and total pFe concentrations of < 0.5 nM, with roughly 50% found in the labile phase, and by highly variable $\delta^{56}Fe_{labile}$ values, with 80% in the range of − 0.5 to + 0.2‰ (n = 169). Below the hydrothermal and OMZ plumes, benthic nepheloid layer labile pFe had similar $\delta^{56}Fe_{labile}$ to particles in the overlying water column features, suggesting that Fe isotopes in surface sediments may be a tracer for the location of active hydrothermal venting and oxygen minimum zones in the past ocean.

Highlights

► Concentration and isotope ratios of labile particulate iron are presented. ► Hydrothermal plume Fe consists of isotopically light Fe oxyhydroxides. ► Isotopically light labile particle Fe observed at top of oxygen minimum zone ► Benthic nepheloid layer labile Fe isotopes reflect those of the features above.

1. Introduction

The role played by iron in biochemical electron transport during photosynthesis and respiration, and within enzymes involved in nitrogen acquisition, makes it an essential micronutrient (Morel et al., 2004). Although iron is the fourth most abundant element in the Earth's crust, low solubility of Fe(III), the thermodynamically stable form in oxygenated waters (Millero, 1998), results in typically subnanomolar concentrations of dissolved iron (dFe) in near-surface oceanic waters (Moore and Braucher, 2008). As a result, low dFe concentrations play a crucial role in setting rates of primary productivity, and iron is the limiting nutrient and/or influences phytoplankton community structure in an estimated 25–50% of the world ocean (Martin et al., 1991; Moore et al., 2004, 2002).

Due to the typically low dFe concentrations in ocean waters, particles also play an important role in the marine biogeochemistry of iron, acting as both a source and a sink for dFe (Boyd and Ellwood, 2010; Lam and Bishop, 2008). This particulate iron (pFe) includes lithogenic, biogenic and authigenic phases, which have different sources, biogeochemistry and degrees of bioavailability (Berger et al., 2008; Boyd et al., 2010; Kuss and Kremling, 1999). Sources of pFe to the ocean include atmospheric deposition to surface waters, resuspension and transport of particles from continental margins, and in situ formation of amorphous Fe oxyhydroxides when soluble Fe(II) is oxidized to insoluble Fe(III) following its release from reducing sediments or hydrothermal vents (Jickells et al., 2005; Lam et al., 2006; Severmann et al., 2010; Statham et al., 2005). Biological uptake of iron followed by sinking of non-living organic material represents a loss of biologically available pFe from surface waters, and is exacerbated by smaller Fe-containing particles being trapped within sinking aggregates or by precipitation and scavenging of dFe onto sinking particles (Bowie et al., 2001; Frew et al., 2006). However, iron within phytoplankton cells and detrital organic material is a viable source for heterotrophs, and rapid recycling of biogenic pFe in surface waters can help sustain biological production (Boyd and Ellwood, 2010; Strzepek et al., 2005).

Iron stable isotope measurements represent a useful tool to investigate sources and fluxes of iron to the ocean (Abadie et al., 2017; Conway and John, 2015, 2014; Labatut et al., 2014; Radic et al., 2011). Distinct iron isotopic compositions are associated

with iron from lithogenic and hydrothermal sources (Beard et al., 2003), and with dFe released from reducing, versus non-reducing sediments (Homoky et al., 2013; John et al., 2012; Severmann et al., 2010). Numerous studies have examined iron isotope fractionation associated with processes that take place within the ocean, including oxidation, reduction, adsorption, dissolution and biological uptake (e.g. Dauphas and Rouxel, 2006; Dideriksen et al., 2008; Staubwasser et al., 2013, 2006), and during mixing of hydrothermal vent fluids with seawater (Bennett et al., 2009; Klar et al., 2017; Rouxel et al., 2016; Severmann et al., 2004).

Over the past decade, stable isotope techniques have been refined to the point where they are practical for making iron isotope measurements (δ^{56}Fe) at the low iron concentrations typical of ocean waters (Conway et al., 2013; John and Adkins, 2010; Lacan et al., 2008). The application of these techniques to filtered seawater samples has demonstrated both regional and depth-related variability in dissolved iron δ^{56}Fe (John et al., 2012; John and Adkins, 2012; Lacan et al., 2008). Furthermore, the combination of iron isotope analyses of end-members (hydrothermal vent fluids, aerosols, sediment pore waters) with basin-scale transects of dissolved δ^{56}Fe has allowed estimates of the fractional contribution of different Fe sources to seawater dFe, proving to be a useful tool in studying biogeochemical cycling of iron in the marine environment (Conway and John, 2014).

Stable isotope studies of marine particulate iron must contend with different forms of pFe, not all of which are available for exchange with seawater or biologically available over the residence time of particles in the surface ocean. Some treatments use a mixture of strong acids to break down the crystalline matrix of refractory material within samples, prior to measuring total particulate δ^{56}Fe (e.g. Bennett et al., 2009; Radic et al., 2011). To assess δ^{56}Fe of the labile fraction of marine particulate material, one must first consider how well any iron released into solution by a given treatment represents biologically available pFe (i.e. "labile" pFe is operationally defined), and secondly, whether the specific conditions of the treatment are likely to bias the δ^{56}Fe of the iron released into solution, through isotope fractionation effects during dissolution.

The oxalate-EDTA leach described by Tovar-Sanchez et al. (2003) was designed as a trace metal clean technique to access only iron adsorbed to particle surfaces,

allowing differentiation between interior biological and exterior scavenged pFe in natural marine particulate samples. More recently, this leach has been adapted to access cellular material, resulting in a treatment that is thought to release into solution both biogenic pFe and authigenic Fe oxyhydroxides, with minimal fractionation of Fe isotopes compared to acid-based leach techniques (Revels et al., 2015a, 2015b). This makes it a suitable method for measuring δ^{56}Fe of "ligand-leachable" pFe associated with natural marine particles.

Here we present concentrations and iron stable isotope data of labile pFe, obtained by applying the same leach to samples collected along the entire US GEOTRACES East Pacific Zonal Transect. We compare the data to similar measurements made in the North Atlantic, and to dFe data from the same Pacific section, and we discuss in more detail what the pFe data can tell us about iron biogeochemistry near the Peruvian margin, and within hydrothermal plumes and benthic nepheloid layers.

2. Methods

2.1 Sample collection

The US GEOTRACES GP16 East Pacific Zonal Transect (hereinafter referred to as GP16) was carried out on RV *Thomas G. Thompson* in October-December 2013, between Manta, Ecuador and Papeete, Tahiti (Fig. 1). The section stretched from high productivity shelf waters and the extensive oxygen minimum zone (OMZ) of the Peruvian Margin upwelling region in the east, to oligotrophic conditions at the western end of the transect. Stations were selected to include sampling close to the Southern East Pacific Rise (SEPR) ridge-axis, at ~15°S, 113°W (Station 18) and along the hydrothermal plume extending over 4000 km westward from there, as previously identified by [3]He analyses (Lupton and Craig, 1981).

Size-fractionated samples (>51 µm and 0.8–51 µm) of particulate material were collected using battery powered McLane in situ pumps, as described elsewhere (Heller et al., 2017; Ohnemus and Lam, 2015). Depth profiles were carried out at four shelf/slope stations (Stations 2–5), 13 full stations, and five superstations (Stations 1, 11, 18, 26 and 36), and involved deployments of between five and eight pumps at shelf/slope stations,

16 pumps (two casts of eight pumps) at full stations or 24 pumps (three casts of eight pumps) at superstations. Samples for trace metal analyses were collected on paired 142 mm diameter 0.8 μm polyethersulfone (Supor) filters loaded underneath a 51 μm polyester mesh prefilter, through which 300–500 L of seawater were typically pumped, following the recommendations of a study into in situ pump sampling methods (Bishop et al., 2012). Only the 0.8–51 μm size fraction is discussed here, and only the upper 0.8 μm filter was processed for both labile and total pFe concentrations, meaning that the 0.2–0.8 μm size fraction was likely under-sampled. However, comparison of upper and lower filter labile pFe concentrations for 25 samples indicate that on average the material from the backing filter contributed <5% of labile pFe. Subsamples of each 0.8 μm filter pair were cut using a ceramic rotary blade, with $1/16^{th}$ of the upper 0.8 μm filter treated with the oxalate-EDTA leach and separate $1/16^{th}$ or $1/8^{th}$ subsamples subjected to a total digest procedure.

2.2 Leach procedure and sample purification

The oxalate-EDTA leach solution was prepared as described in Revels et al. (2015a) and cleaned before use, to lower the Fe concentration, by addition of hydroxylamine, perchlorate and 1,10-phenanthroline and extraction of the resulting ferrous ion complex into 1,2-dichloroethane (Tovar-Sanchez et al., 2003). All plasticware used was rigorously acid cleaned prior to use, following Conway et al. (2013), and high purity acids, obtained by sub-boiling distillation in quartz (hydrochloric acid) or Teflon PFA (nitric acid) stills, were used. All sample processing was carried out in flow benches with ultra low particulate air (ULPA) filtration, in a clean air laboratory at the University of South Carolina.

Application of the leach was similar to that described in Revels et al. (2015a). Each filter section was loosely folded and sealed in a 2 mL polyethylene vial (Nalgene) with 1 mL of oxalate-EDTA leach solution and heated at 90°C for two hours. The leachate was subsequently transferred to a 3 mL polyethylene/polypropylene syringe (Norm-Ject) and filtered through a 4 mm polypropylene syringe filter with 0.45 μm PTFE membrane (Whatman) into a clean 2 mL vial. Multi-element concentration analyses were

carried out on a Thermo-Element II sector field inductively coupled plasma mass spectrometer (ICP-MS) at the University of South Carolina Center for Elemental Mass Spectrometry (CEMS). Concentration samples were prepared by diluting an aliquot of the leachate to 5% of original concentration with 0.1 M HNO_3 and measuring signal intensity relative to matrix-matched standards, prepared by diluting the oxalate-EDTA solution to 5% concentration with 0.1 M HNO_3. All samples, blanks and standards were prepared containing 10 ppb In as an internal standard.

Following concentration analysis, aliquots of each leachate, typically containing 75 ng of Fe, were transferred to 7 mL Teflon PFA vials. For some samples, low Fe concentration within the leachate meant that a smaller amount of Fe had to be used. Each sample was spiked with an Fe double-spike solution, containing roughly equal amounts of ^{57}Fe and ^{58}Fe, to give a 1:2 natural-to-spike Fe ratio. These spiked samples were evaporated to dryness, then reacted with 150 μl of concentrated HNO_3 and 150 μl of concentrated H_2O_2 at 200°C for 2.5 hours to digest organic material in the leachate, before being dried down a second time. Samples were then reconstituted in 200–600 μl of 10 M HCl with 0.01% v/v H_2O_2 and purified by anion exchange chromatography. Following Conway et al. (2013), samples were loaded onto columns of AG-MP1 resin and, after first eluting salts and Cu from the columns, Fe was eluted with 800 μl of 1 M HCl and collected in clean Teflon PFA vials. Samples were then dried down and reconstituted in 1.5 mL of 0.1 M HNO_3 for isotopic analysis.

Although no certified reference materials were treated with the leach reagent in this study, applications of the procedure to duplicate aliquots of MESS-3 (marine sediment, National Research Council of Canada) and two other natural particulate samples (Cariaco Basin sediments and Arizona Test Dust) during method development showed 5–10% reproducibility of concentration data (Revels et al., 2015b).

2.3 Iron stable isotope analysis

Iron stable isotope ratios were measured at CEMS using a Thermo Neptune multi-collector ICP-MS, following established methods (Conway et al., 2013; Revels et al., 2015a). Samples were introduced at a concentration of 50 ppb sample and 100 ppb Fe

double-spike (occasionally lower due to low concentrations of leachable Fe in the filtered material) using an ESI Apex-Q introduction system without a desolvating membrane. Instrumental bias was corrected using the double-spike, and [53]Cr and [60]Ni were monitored in order to correct for isobaric interferences from Cr and Ni.

The Fe stable isotope ratios are reported in delta notation, relative to the IRMM-014 isotope standard, such that:

$$\delta^{56}Fe_{sample}\ (‰) = \left(\frac{(^{56}Fe/^{54}Fe)_{sample}}{(^{56}Fe/^{54}Fe)_{IRMM-014}} - 1 \right) \times 1000 \qquad (1)$$

The internal analytical error (2σ) for δ^{56}Fe ranged from 0.02 ‰ for most samples, introduced at 50 ppb sample concentration, to 0.10 ‰ for a small number introduced at 5 ppb sample concentration. In addition, the double-spike method gives a very accurate measurement of the sample/spike ratio of samples. As a result, labile pFe concentrations reported here are determined from isotopic analyses, rather than the initial measurements made on the Thermo Element ICP-MS.

2.4 Leach reagent blanks and filter blanks

Two batches of the oxalate-EDTA reagent were prepared. The first contained 13.3 ± 0.2 ng g^{-1} Fe, with δ^{56}Fe of –5.37 ± 0.06 ‰ (mean ± 1σ, n=4), and was used for all samples and dipped filter blanks except those from Stations 25, 28, 30, 32 and some from Station 23. The second batch, used for the remaining samples and blanks, contained 122.4 ± 0.8 ng g^{-1} Fe, with δ^{56}Fe of –4.99 ± 0.07 ‰ (n=4) (Table 1). Leach reagent blank corrections were made to all samples and dipped filters. This represented a significantly higher fraction of measured concentrations for samples and filter blanks leached with the second batch of reagent (Table 1), though the excellent precision of leach blank replicates meant that it contributed little to the overall uncertainty in calculated sample concentrations.

In addition, an average dipped filter blank was calculated at 7.5 ± 4.4 ng g^{-1} (n=34), equivalent to a labile pFe concentration of ~2.1 nmol/filter, or ~0.01 nM, based on typical volumes filtered. The limit of detection calculated from propagated standard

deviations of reagent and dipped filter blanks was calculated at ~0.02 nM for both reagent batches, based on typical volumes filtered, with most of this due to variations in dipped filter blanks. All but one blank-corrected samples had concentrations above this limit of detection. With the reagent blank and dipped filter blank well quantified, uncertainty in measured labile pFe concentrations is dominated by the uncertainty associated with the leach procedure itself, which ranges from 5–10%, based on treatments of replicate natural particulate samples (Revels et al., 2015b).

The dipped filter blanks were not used to correct sample δ^{56}Fe values, due to low Fe concentrations and the low volume of leachate available. Instead, following Revels et al. (2015a), reagent blank δ^{56}Fe corrections were made to measured values using the isotopic mass balance equation:

$$\delta^{56}Fe_S = \frac{\delta^{56}Fe_M \times [Fe]_B + \delta^{56}Fe_M \times [Fe]_S - \delta^{56}Fe_B \times [Fe]_B}{[Fe]_S} \qquad (2)$$

where S, M and B represent sample, measured and blank values, and [Fe] represents iron concentration of the leachate. Uncertainties in δ^{56}Fe reported here are propagated from 2σ internal error of sample analyses and uncertainties in the reagent blanks.

Labile pFe concentrations are reported here as nanomolar concentrations, based on blank corrected leachate Fe concentration, the fraction of filter used and the volume of seawater pumped through the filter. All ligand-leachable pFe concentration and δ^{56}Fe data are publicly available at the Biological and Chemical Oceanography Data Management Office (BCO-DMO) online data repository (www.bco-dmo.org/dataset/669178)

2.5 Total digest procedure

Separate subsamples of the top Supor filter, representing 1/16th or 1/8th of the filter area (about 25–50 L equivalent volume filtered), were digested in a HEPA-filtered venting fume hood at the University of California, Santa Cruz (UCSC), for determination of total particulate trace metal concentrations in the 0.8–51 μm size fraction (Heller et al.,

2017; Lee et al., this issue). Briefly, the polyethersulfone filter was first completely dissolved in the highly oxidizing Piranha reagent (3:1 $H_2SO_4:H_2O_2$), and then particles, including lithogenic material, were dissolved in a strong acid mixture containing 4 M each of HNO_3, HCl and HF (Ohnemus et al., 2014; Ohnemus and Lam, 2015). After drying down, the final remaining droplet was brought up in 2 mL 5% HNO_3 with 1 ppb In as an internal standard, and analyzed on a Thermo Scientific Element XR ICP-MS in the UCSC Plasma Analytical Facility. The median dipped blank filter was subtracted from all samples. Regular application of this procedure to two certified reference materials gave Fe recoveries of $106 \pm 8\%$ (mean $\pm 1\sigma$; $n=12$) for BCR-414 (freshwater plankton) and $84 \pm 6\%$ ($n=12$) for PACS-2 (coastal marine sediment) (Heller et al., 2017; Lee et al., this issue).

Uncertainty in the total pFe concentration was typically dominated by uncertainty in the dipped blank filter subtraction (14%), followed by that from repeat analyses (5%). The detection limit, defined as three times the standard deviation of dipped blank filters, was 54 nmol/filter, which translates to a detection limit of 0.14 nM, given typical volumes filtered. The significantly higher detection limit and filter blank subtraction, relative to those for the labile pFe dipped filter blank, is largely due to digestion of the filter matrix.

3. Results

3.1 Labile pFe concentration and isotopic composition

Concentrations of labile particulate iron, [Fe_{labile}], spanned four orders of magnitude (0.01–42.0 nM; $n=341$). Median [Fe_{labile}] was 0.19 nM and 79% of all samples had [Fe_{labile}] <1 nM (Fig. 2a, 3). Highest concentrations were measured in samples collected from a neutrally buoyant hydrothermal plume near the SEPR, at Stations 18 and 20, which included the only samples with [Fe_{labile}] above 10 nM. Elevated [Fe_{labile}] of >1 nM was associated with the plume at all stations as far as Station 28, with a weaker plume signal still evident as far as Station 36. Near the Peruvian margin, [Fe_{labile}] of >5 nM was detected in the upper 500 m at Station 1 and the shelf/slope stations, 2–5.

Elevated [Fe_{labile}] was also measured within benthic nepheloid layers at several stations (Fig. 2a, 3).

The iron stable isotope signature of labile pFe, $\delta^{56}Fe_{labile}$, ranged from −1.39 ‰ to +0.96 ‰ (Fig. 2c, 4), with a mean (± 1σ) value of −0.35 ± 0.31 ‰ (*n*=341). The majority (89%) of samples had $\delta^{56}Fe_{labile}$ below 0 ‰. At each station, $\delta^{56}Fe_{labile}$ was generally more variable in the upper 1000 m than in the deep ocean (Fig. 4).

3.2 Total pFe concentration

Concentrations of iron measured following the total digest method, [Fe_{total}], also spanned four orders of magnitude, from 0.01−34.6 nM, with a median value of 0.35 nM. Despite the large range, 78% of samples had [Fe_{total}] <1 nM. As for [Fe_{labile}], the highest concentrations were associated with the SEPR hydrothermal plume (Fig. 2b). Most samples from Stations 1−5, closest to the Peruvian margin, also had [Fe_{total}] of >1 nM, as did a few samples collected from benthic nepheloid layers along the section.

Using [Fe_{labile}] and [Fe_{total}] for each sample, we calculated the fraction of total pFe present in labile phases, f_{labile} (=[Fe_{labile}]/[Fe_{total}]; Fig. 2d). In some cases, the calculated f_{labile} was >1, due to analytical uncertainties, heterogeneous particle distribution on filters, and a dominant [Fe_{labile}] contribution to [Fe_{total}] (see Section 4.1.2).

Digest samples from Stations 26 and 36 were subjected to the same Fe double-spike addition and anion exchange chromatography purification process described for leach samples (see Methods), and analyzed for stable iron isotope ratios ($\delta^{56}Fe_{total}$). This small dataset showed less variability than the more numerous $\delta^{56}Fe_{labile}$ data, with values ranging from −0.36 ‰ to +0.40 ‰ (Fig. 5), and a mean (± 1σ) of +0.06 ± 0.20 ‰ (*n*=47).

4. Discussion

4.1 General features of pFe along the GP16 transect

4.1.1 Labile and total pFe concentrations

In order to compare different aspects of the GP16 section, we split the data into different sub-divisions (Table 2). These include samples collected from the OMZ in the

eastern part of the transect, defined by dissolved oxygen concentrations of <20 μmol kg^{-1}, and from the hydrothermal plume that spreads westward from the SEPR. For the purposes of this study, we define plume samples as those collected between 2200–3000 m at stations west of and including Station 18, which coincides roughly with the 75 fmol kg^{-1} excess ^{3}He contour (Fig. 2). We divide the rest of the data into subsets east (Stations 1–17) and west (Stations 18–36) of the SEPR, and further split between deep (>100 m depth) and surface (<100 m depth) ocean, the latter of which includes all surface mixed layer and deep chlorophyll maximum (DCM) samples. A small number of samples are defined as benthic nepheloid layer (BNL) samples when [Fe$_{labile}$] and [Fe$_{total}$] profiles show an increase with depth within 500–1000 m of the seafloor.

The distributions of [Fe$_{total}$] and [Fe$_{labile}$] varied in similar ways across the entire GP16 dataset (Fig. 6), and over the entire section, median [Fe$_{total}$] was almost double that of [Fe$_{labile}$], at 0.35 nM, compared to 0.19 nM. Both [Fe$_{labile}$] and [Fe$_{total}$] were highest in the SEPR hydrothermal plume and near the Peruvian margin, and lower for samples more distant from these sources of pFe input (Fig. 2a,b, Table 2). Excluding hydrothermal plume and OMZ samples, deep ocean [Fe$_{labile}$] values were typically lower in the western part of the section (Table 2), a characteristic shared by dFe distributions along GP16 (Fig. 7). The lowest average concentrations of iron were measured in surface waters, where median [Fe$_{labile}$] was <0.1 nM, while BNL [Fe$_{labile}$] and [Fe$_{total}$], where sampled, were elevated over deep ocean values.

The concentration ranges of [Fe$_{labile}$] and [Fe$_{total}$] observed during this study were similar to those measured during the US GEOTRACES North Atlantic (GA03) section, although maximum and median concentrations of each were higher for GA03 (Revels et al., 2015a) and concentrations of <0.1 nM were more widespread along GP16. This is likely due to differences in section placement and biogeochemical considerations, including greater atmospheric inputs of pFe along GA03 compared to GP16 (Jickells et al., 2005; Mahowald et al., 2005), and the fact that GA03 was a full basin transect, with margin influences at each end (Ohnemus and Lam, 2015).

4.1.2 Fraction of labile pFe

It is apparent from Fig. 2d that f_{labile} was calculated at >1 for a small number of GP16 samples (~15 % were >1, though only nine samples had f_{labile} of >1.5), suggesting an overestimation of [Fe$_{labile}$] or underestimation of [Fe$_{total}$]. These instances are likely due to a combination of the level of precision of ICP-MS measurements of both samples and filter blanks, to uncertainties in the exact size of filter fraction used for each analysis, to uneven filter loading during sample collection, and to the precision of the leaching procedure. Replicate analyses carried out on natural particles suggest that the latter represents a 5–10% error in [Fe$_{labile}$] (Revels et al., 2015a). For [Fe$_{total}$] measurements the greatest uncertainty at low concentrations was in the blank filter subtraction. At high Fe concentrations, where blank subtraction was negligible, the discrepancies in f_{labile} are likely due to heterogeneity of particle distribution on filters, as leach and digest procedures were carried out on different filter sections. As discussed by Bishop et al. (2012), heterogeneity in particle distribution typically increases with sample depth, as the fraction of sticky organic matter decreases. Images of filters taken at sea confirm that some samples, particularly those from deeper in the water column, had poor particle distribution (Fig. S1).

Despite the uncertainty associated with calculating f_{labile}, some notable features are apparent (Fig. 2d, Table 2). Samples collected from the hydrothermal plume and from the OMZ had f_{labile}≈1, indicating that pFe from each was readily dissolved by the oxalate-EDTA leach. The influence of the OMZ and shelf-derived labile pFe is also evident in deeper waters for the eastern part of the section, which had generally higher f_{labile} values compared to those further west (median of 0.7, compared to 0.5). Particles collected close to the seafloor often had relatively low f_{labile}, notably those from stations near the Peruvian margin (see Section 4.4).

Somewhat surprisingly, f_{labile} values for samples collected in the DCM, which varied from 6–38 m depth on the shelf to 45–95 m further west, averaged only 0.5, though they ranged from 0.1–1. As the leach treatment is designed to extract iron associated with cellular and detrital biological material it might be expected that samples from the DCM would be close to 1 (Revels et al., 2015a). That this was not always the case may be a result of the very low surface ocean pFe concentrations, resulting in greater relative uncertainty following blank subtractions for both [Fe$_{labile}$] and [Fe$_{total}$]. Values of

[Fe$_{labile}$] were <0.1 nM for all DCM samples west of Station 1, while several DCM blank-corrected [Fe$_{total}$] values were below the detection limit of 0.14 nM. In addition, higher [Fe$_{total}$] for DCM samples at Stations 34 (0.38 nM at 45 m) and 36 (0.19 nM at 75 m) may indicate contributions of lithogenic material from dust deposition, from material carried eastwards in the Equatorial Undercurrent (Radic et al., 2011), or from material originating from islands to the north or south of the western end of the section (Fig. 1).

4.1.3 Particulate δ^{56}Fe

   Ligand-leachable pFe was generally isotopically light compared to continental material ($\delta56$Fe ~ 0 ‰; Beard et al., 2003) and was also light compared to dissolved iron (δ^{56}Fe$_{diss}$) throughout the GP16 section (Fig. 2c, 7). Lightest values of δ^{56}Fe$_{labile}$ were found at the eastern end of the section (Table 2), with a median of −0.71 ‰ for Stations 1−9, compared to −0.30 ‰ for Stations 11−30 and −0.11 ‰ for Stations 32−36. This pattern follows the distribution of δ^{56}Fe$_{diss}$ along the section, which was typically light in the eastern half and heavy in the western half (John et al., this issue). The trend in δ^{56}Fe$_{labile}$ is evident in both surface and deep waters (Table 2) and the distribution of δ^{56}Fe$_{labile}$ (and δ^{56}Fe$_{diss}$) likely represents a decreasing influence from east to west of isotopically light Fe derived from reducing sediments (Chever et al., 2015; Severmann et al., 2006), a greater relative contribution from atmospheric deposition farther from the margin (Beard et al., 2003; Labatut et al., 2014) and a greater influence (at depth) in the west from hydrothermal iron (Fitzsimmons et al., 2017). The release of heavier dFe (~+0.2 ‰) from non-reducing sediments to the deep ocean and to near-surface waters around nearby islands likely also contributes to heavier δ^{56}Fe$_{labile}$ and δ^{56}Fe$_{diss}$ values farther west (Homoky et al., 2013; Radic et al., 2011).

   The greater variability in δ^{56}Fe$_{labile}$ observed throughout the upper 1000 m (Fig. 4) is partly due to the lower concentrations measured, resulting in less Fe in samples for isotope measurements and so lower precision, as indicated by larger error bars (e.g. Stations 28 and 30). More significantly, the upper few hundred meters are associated with more processes that may affect stable isotope composition of labile pFe, such as photochemical reduction and subsequent oxidation, biological uptake, release of dFe during remineralization of organic material, precipitation of Fe oxyhydroxides, and

partial dissolution of iron associated with atmospheric dust (Dideriksen et al., 2008; Ellwood et al., 2015; John and Adkins, 2012; Radic et al., 2011).

At two stations where isotope analyses were carried out on total particle digest samples, the median difference between $\delta^{56}Fe_{labile}$ and $\delta^{56}Fe_{total}$ ($\Delta\delta^{56}Fe_{labile-total}$) was −0.15 ‰ (Fig. 5). This is smaller than the average $\Delta\delta^{56}Fe_{labile-total}$ of −0.39 ‰ observed for the GA03 section (Revels et al., 2015a), which may simply be due to the smaller $\delta^{56}Fe_{total}$ dataset available from GP16, but may also reflect biogeochemistry at the two stations for which it was measured. Labile pFe contributed a greater fraction to total pFe at GP16 stations 26 and 36 (median f_{labile} = 0.5, n=50) than on average during GA03 (median f_{labile} = 0.3, n=175). Comparison of $\delta^{56}Fe$ depth profiles shows distinctly lighter values of $\delta^{56}Fe_{labile}$ and particularly $\delta^{56}Fe_{total}$ at 2200–3000 m depth at Station 26 (Fig. 5b) than at Station 36 (Fig. 5d) due to the greater influence of hydrothermal iron at the former (Fig. 5a,c).

The predominantly light $\delta^{56}Fe_{labile}$ values, relative to those of $\delta^{56}Fe_{diss}$ throughout the GP16 section (Fig. 7) indicate that any transfer between the two phases preferentially partitions heavier isotopes to the dissolved fraction and/or lighter isotopes in the labile particulate fraction. This was true both in the western part of the section, where $\delta^{56}Fe_{diss}$ was heavier than crustal values, and within the plume of elevated Fe concentrations extending from the Peruvian margin (John et al., this issue), and was also observed throughout the GA03 section (Conway and John, 2014; Revels et al., 2015a), suggesting a widespread phenomenon. One potential mechanism for this is preferential precipitation as oxyhydroxides and/or scavenging of isotopically light Fe, leaving behind heavier dFe. This is consistent with the observed isotopically heavy dFe within the OMZ, despite much lighter values close to the reducing sedimentary source (John et al., this issue).

4.2 Hydrothermal plume Fe$_{labile}$

Highest [Fe$_{labile}$] and [Fe$_{total}$] values were measured in plume samples at Station 18, closest to the vent site on the SEPR (Fig. 2a,b, 3), which also yielded the highest concentrations along the section for dFe and pFe from GO-FLO bottle samples (Fitzsimmons et al., 2017; Resing et al., 2015). At Stations 18 and 20, within ~100 km of

the ridge axis, f_{labile} values of ~1, indicate that essentially all of the plume pFe was labile. Analysis of plume particulate material revealed that up to 60% of total mass in the small size fraction consisted of newly precipitated Fe oxyhydroxides (Fitzsimmons et al., 2017; Lam et al., this issue), which are known to form near hydrothermal vents as dFe in hot, anoxic hydrothermal fluid mixes with cold, oxygenated sea water (Rudnicki and Elderfield, 1993).

For near-field hydrothermal samples, the dFe and labile pFe isotope ratios were indistinguishable within analytical error, with $\delta^{56}Fe_{labile}$ of -0.25 ± 0.08 ‰ ($n=22$) compared to $\delta^{56}Fe_{diss}$ for Station 18 of -0.19 ± 0.05 ‰ ($n=4$). This suggests that the only difference between pFe and dFe in the near-field neutrally buoyant plume is size – a mixture of particulate and colloidal-sized inorganic Fe(III) oxyhydroxides (Fitzsimmons et al., 2017). Although no vent fluid samples were collected during GP16, near-field $\delta^{56}Fe_{labile}$ and $\delta^{56}Fe_{diss}$ both fall within the range of $\delta^{56}Fe$ values measured for high temperature vent fluids (-0.2 ‰ to -0.6 ‰) at various sites in the Pacific and North Atlantic oceans (Beard et al., 2003; Bennett et al., 2009; Klar et al., 2017; Rouxel et al., 2016; Severmann et al., 2004). We therefore speculate that the near-field $\delta^{56}Fe_{labile}$ closely resembles the iron isotope signature of the vent fluid end-member at the SEPR vent from which the plume originated.

Severmann et al. (2004) interpreted the similarity between $\delta^{56}Fe$ of neutrally buoyant plume particles originating from a North Atlantic vent and those of the vent fluid as near-quantitative mass conservation as vent fluid Fe(II) was oxidized to form Fe(III) oxyhydroxides by the time the plume had become neutrally buoyant. Our $\delta^{56}Fe_{labile}$ and $\delta^{56}Fe_{diss}$ also match the -0.19 ± 0.09 ‰ calculated by Bennett et al. (2009) specifically for Fe oxyhydroxide particles formed in a buoyant plume on the Mid-Atlantic Ridge. This is supported by only a minor contribution from Fe(II) minerals to pFe in plume samples at Stations 18 and 20 during GP16 (Fitzsimmons et al., 2017). There is therefore no evidence in our $\delta^{56}Fe_{labile}$ data of the variability associated with early (buoyant) plume dynamics, attributed to Fe-sulfide formation, and Fe-oxyhydroxide precipitation from partial Fe(II) oxidation (Klar et al., 2017; Rouxel et al., 2016; Severmann et al., 2004).

Westward from the SEPR, maximum plume [Fe_{labile}] dropped significantly from 42 nM at Station 18 to 6.9 nM at Station 21, some 120 km further west, mirroring the loss

of [Fe_{total}] (Fig. 2a,b). Values of f_{labile} remained at ~1. This loss is attributed to near-field self-aggregation of plume particles to form larger particles that then sink to the seafloor (Fitzsimmons et al., 2017). An apparent break in the pFe plume at Station 23, with maximum [Fe_{labile}] of <1 nM, is probably due to a meridional circulation feature shifting the core of the plume slightly to the north of the transect (Jenkins et al., this issue), as peak [Fe_{labile}] was back up to 2.6 nM at Station 25, and then decreased more gradually with distance further west until becoming barely distinguishable from background concentrations by Station 36 (Fig. 2a, 3). Values of [Fe_{total}] within the plume showed a similar pattern (Fig. 2b). Peak concentrations within the plume of both labile and total pFe gradually deepened along the section, from 2450 m at Station 18 to 2800 m at Station 32, due to the relatively dense Fe oxyhydroxide particles being embedded within low specific gravity organic matter (Fitzsimmons et al., 2017).

Despite the significant decrease in [Fe_{labile}] along the plume, values of $\delta^{56}Fe_{labile}$ varied little, averaging -0.26 ± 0.14 ‰ for all plume samples (n=67) and ranging from -0.25 ± 0.08 ‰ at Stations 18 and 20 to -0.38 ± 0.07 ‰ at stations 21−28, and -0.15 ± 0.14 ‰ at stations 30−36. This is consistent with the loss of plume pFe occurring mainly by physical processes (aggregation into larger, sinking particles or reversible scavenging), rather than chemical reactions, which would be expected to result in larger changes in $\delta^{56}Fe$ (e.g. Dauphas and Rouxel, 2006).

Plume values of f_{labile} remained close to 1 as far as Station 28 (Fig. 2d), and at Station 26, $\delta^{56}Fe_{total}$ data for plume samples were almost identical to $\delta^{56}Fe_{labile}$ (Fig. 5b). A similar observation was made from samples from the TAG plume during GA03 (Figure 8 of Revels et al., 2015a). Westward of Station 28, plume f_{labile} decreased to ~0.6 by Stations 32 and 34, and ~0.5 by Station 36, similar to the values measured in the water column above the plume. This is partly due to plume [Fe_{labile}] decreasing to deep ocean background concentrations at the westernmost stations (Fig. 2d, 3), but also due to an increasing contribution to [Fe_{total}] at plume depths from lithogenic material in this portion of the transect. This material may originate from subsurface sources of lithogenic material, such as the Tuamotu Plateau (south of Stations 32−36, at ~15°S) or around the Marquesas Islands (north of the transect between Stations 30−32), or it may be a result of slightly higher atmospheric dust deposition at the western end of the transect, relative to

Stations 13−25 (Lam et al., this issue; Lee et al., this issue). This may also explain the larger offset between $\delta^{56}Fe_{labile}$ and $\delta^{56}Fe_{total}$ measured in deep samples at station 36 (Fig. 5d), where values of the latter were close to the ~0 ‰ of lithogenic material (e.g. Beard et al., 2003).

4.3 Peruvian Margin Fe$_{labile}$

The Peruvian margin portion of the GP16 section encompassed shelf, slope and open ocean stations, and included samples collected above, within and beneath the South Pacific OMZ. The OMZ results from sluggish circulation, combined with high oxygen demand due to intense degradation of organic matter in the highly productive upwelling regime along the Peruvian/Chilean coastline, and stretches as far as ~37°S from the equator and reaches ~140°W at its greatest extent (Fuenzalida et al., 2009). Along the GP16 section the OMZ extended as far west as Station 13. On the shelf it extended from 20 or 30 m depth to the seafloor, and the upper oxycline gradually deepened offshore from east to west. The vertical extent was greatest (~700 m thick) at slope and offshore Stations 5 and 1, and gradually thinned with distance further offshore (Fig. 2). The Peruvian margin sampling also revealed evidence of material apparently resuspended from slope sediments beneath the OMZ.

4.3.1 Fe$_{labile}$ and $\delta^{56}Fe_{labile}$ within the OMZ

Stations 2, 3 and 4, on the Peruvian shelf and upper slope, each had near-seafloor concentration maxima for total dFe and dFe(II) (Heller et al., 2017; John et al., this issue), in line with previous Peruvian shelf observations (Hong and Kester, 1986; Noffke et al., 2012; Scholz et al., 2014a, 2011). The dFe maxima are likely due to diffusion into the low oxygen water column, from sediment porewaters, of isotopically light dFe(II) formed by dissimilatory iron reduction of reactive Fe oxyhydroxides in the sediments (Burdige, 1993; Severmann et al., 2006). Although at Station 2, $\delta^{56}Fe_{diss}$ was isotopically light and dFe(II) accounted for the majority of total dFe throughout the OMZ, at Stations 3 and 4, $\delta^{56}Fe_{diss}$ was ~0 ‰ throughout the OMZ except close to the seafloor (John et al.,

this issue) and the percentage dFe(II) contribution to total dFe decreased with height above the seafloor (Heller et al., 2017).

Each station also had elevated [Fe$_{labile}$] throughout the water column (Fig. 3), with highest concentrations in the upper part of the OMZ, coincident with maxima in nitrite concentration (Heller et al., 2017) Values of f_{labile} were ~1 and, with one exception (see below), Fe$_{labile}$ was isotopically light, averaging −0.71 ± 0.20 ‰ (n=16), and similar to previous values inferred for Peruvian shelf pFe from differences in δ^{56}Fe between filtered and unfiltered samples (Chever et al., 2015).

Oxygen minimum zone δ^{56}Fe$_{labile}$ was similarly light in off-shelf waters, averaging −0.70 ± 0.28 ‰ (n=28), while [Fe$_{labile}$] was generally lower than on the shelf. However, a subsurface [Fe$_{labile}$] maximum, coincident with the secondary nitrite maximum (SNM), persisted offshore as far west as Station 13, decreasing from 7.3 nM at Station 5 to 0.32 nM at Station 13 (Fig. 3), and this pattern was paralleled by [Fe$_{total}$] (Fig. 2c). The depth of this maximum increased as the SNM deepened, from ~65 m on the shelf to ~250 m by Station 13, following the deepening of the 26.1−26.55 kg m^{-3} density surfaces. A similar persistence of measurable dFe(II) concentrations within the SNM (Heller et al., 2017) mirrored previous observations from the Peruvian margin and has also been observed in the Arabian Sea OMZ (Kondo and Moffett, 2015; Moffett et al., 2007; Vedamati et al., 2014). Throughout the off-shelf OMZ, f_{labile} remained high (median 0.9; Fig. 2d).

Synchrotron X-ray analyses show the OMZ pFe samples to be dominated by Fe(III) oxyhydroxides, including lepidocrocite (γ-FeO(OH)), indicating that Fe oxidation occurred in the presence of aqueous Fe(II) (Heller et al., 2017). Thus the low δ^{56}Fe$_{labile}$ values suggest that elevated [Fe$_{labile}$] through the OMZ is due to oxidation of light dFe(II) released from reducing sediments as it diffuses through the water column. The observed [Fe$_{labile}$] maxima near the top of the OMZ may be due to mixing of anoxic waters with oxic waters in the upper oxycline, causing greater precipitation of Fe(III) oxyhydroxides (Scholz et al., 2011; Staubwasser et al., 2013). Alternatively, the upper OMZ [Fe$_{labile}$] maxima may represent in situ oxidation of dFe(II) released from anoxic sediments further inshore and transported laterally along isopycnals (Heller et al., 2017). Evidence for lateral transport of dFe(II) comes from the observed correlation between dFe(II) and

excess ^{228}Ra (a tracer of recent diffusion from sediments) (Cutter et al., this issue). Some fraction of the [Fe$_{labile}$] may also represent similar lateral transport of Fe oxyhydroxides formed by the same process further inshore. The offshore persistence of dFe(II), along with elevated [Fe$_{labile}$], within the SNM may reflect dynamic redox cycling of Fe within the SNM, while the coincidence of the features may indicate a non-oxygen-dependent pathway, possibly involving nitrite and/or nitrate (Heller et al., 2017; Scholz et al., 2016).

The one isotopically heavy δ^{56}Fe$_{labile}$ measurement of +0.54 ‰ from the shelf stations, coincident with the [Fe$_{labile}$] maximum at Station 2 (70 m), is consistent with the δ^{56}Fe of "easily HCl-extractable" pFe measured in Peruvian shelf sediments, and may indicate an additional contribution to [Fe$_{labile}$] in that sample from other reactive pFe species, originating from resuspended sediments further onshore (Scholz et al., 2014b). However, we note that synchrotron-determined pFe redox speciation of that sample indicates no obvious differences between it and the samples collected above and below it (55 m and 108 m, respectively) (Heller et al., 2017).

A surprising feature of the OMZ is that, while measured δ^{56}Fe$_{labile}$ was consistently light, δ^{56}Fe$_{diss}$ values were typically >0 ‰, other than at Station 2. The lack of a light δ^{56}Fe$_{diss}$ signal associated with the dFe(II) feature that persists offshore may arise because of the relatively low contribution made by dFe(II) to total dFe as the feature decreases offshore, with the light isotopic signature of dFe(II) being mixed with a heavier dFe(III) signal. The systematically lighter δ^{56}Fe$_{labile}$ values, relative to δ^{56}Fe$_{diss}$, throughout the OMZ may indicate that preferential precipitation and/or adsorption of light Fe isotopes to particles may transfer the light isotopic signature of dFe derived from reducing sediments to the labile particulate phase. This transfer has been described previously in relation to the oxic-anoxic boundary of the Baltic Sea (Staubwasser et al., 2013).

4.3.2 Influence of the OMZ and slope resuspension on deep ocean pFe

The influence of the OMZ was evident in δ^{56}Fe$_{labile}$ and f_{labile} for samples collected throughout the eastern part of the GP16 section (Table 2). Beneath the OMZ at Stations 1−13, δ^{56}Fe$_{labile}$ only slightly heavier than within the OMZ (−0.57 ± 0.17 ‰, n=62), coincided with a plume of isotopically light dFe (−0.5 to 0 ‰) that extended over ~4000

m of the water column at Station 1 and persisted 1000 km from the slope, gradually thinning westward (Fig. 7). Reversible scavenging between light pFe and dFe as it is advected away from the continental margin is thought to be responsible for this plume (John et al., this issue).

Values of f_{labile} in deep waters beneath the OMZ were also generally higher than in the west (Table 2), presumably because of the contribution of labile Fe oxyhydroxides formed in shelf and/or OMZ waters. But they were lower than within the OMZ itself, indicating more heterogeneity in the deep pFe. Elevated [Fe$_{labile}$] and [Fe$_{total}$] in samples from Stations 5 and 1 in particular represent contributions of labile and refractory pFe resuspended from deep slope sediments (Fig. 2a,b, 3). Synchrotron chemical mapping of material from the lower oxycline (1200 m) and below the OMZ (1800 m and 2040 m) at Station 5 demonstrate that low f_{labile} values (~0.3) associated with elevated [Fe$_{labile}$] are due to a greater contribution of crystalline particulate Fe(II) species than for samples collected within the OMZ (Heller et al., 2016). Similarly, a broad secondary subsurface maximum in [Fe$_{labile}$] was centered around 2400 m at Station 1 (~1 nM, with f_{labile} of 0.5), coincident with elevated concentrations of lithogenic material (Lam et al., this issue). However, δ^{56}Fe$_{labile}$ in each case was still isotopically light, suggesting that the labile contribution to pFe was similar to that in the OMZ. This mixture of labile and refractory pFe, apparently originating from the continental slope and transported into the deep ocean (Lam and Bishop, 2008), results in higher average deep ocean [Fe$_{labile}$] concentrations in the eastern part of the section than in the west (Table 2).

4.4 Characteristics of benthic nepheloid layer Fe$_{labile}$

Increases in [Fe$_{labile}$] and [Fe$_{total}$] near the seafloor, associated with BNLs, were evident at several stations, notably Stations 1, 13 and 15 in the eastern half of the transect and Stations 26 and 30 west of the SEPR (Fig. 2a,b 3). While the highest concentrations associated with BNLs along GP16 were at Station 1, where [Fe$_{labile}$] and [Fe$_{total}$] reached 2.8 nM and 5.8 nM, respectively, none were as intense as those encountered in the western North Atlantic during GA03, where [Fe$_{total}$] reached ~1 μM (Ohnemus and Lam, 2015; Revels et al., 2015a).

Nepheloid layer $\delta^{56}Fe_{labile}$ values ranged from -0.89 ‰ to -0.03 ‰, and typically resembled those of prominent $[Fe_{labile}]$ features in the water column above, while BNL f_{labile} values (0.2–1.0, median = 0.5; n=32) revealed a variable contribution from refractory pFe in resuspended near-bottom material (Fig. 2c,d). Indeed, water-column integrated and depth-weighted BNL $\delta^{56}Fe_{labile}$ values were calculated to be, on average, within 0.05 ‰ of those for the overlying water column (Fig. 8a). A similar treatment of f_{labile} values showed greater offsets between BNL and water column values for several stations (Fig. 8b)

Measured BNL $\delta^{56}Fe_{labile}$ from beneath the hydrothermal plume, at stations 25, 26, 28 and 30, averaged -0.34 ± 0.03 ‰ (n=7), statistically the same as that for hydrothermal plume particles (Table 2) and consistent with the labile component of BNL pFe being mainly Fe oxyhydroxides that had settled from the plume. We note that this value is also statistically indistinguishable from the more variable $\delta^{56}Fe_{labile}$ values for non-plume deep ocean samples west of Station 18 (-0.26 ± 0.26 ‰; n=87). However, $[Fe_{labile}]$ for non-plume deep ocean samples was much lower than that for samples within the plume (Fig. 2a, Table 2). Furthermore, at Stations 25 and 26, where depth-integrated $\delta^{56}Fe_{labile}$ values for "plume" (>2200 m) and "non-plume" (<2200 m) samples differed from each other, BNL $\delta^{56}Fe_{labile}$ was closer to the "plume" value (Fig. 8c). Thus, we suggest that BNL $\delta^{56}Fe_{labile}$ in this region is controlled primarily by Fe oxyhydroxide particles that settled from the hydrothermal plume.

BNL f_{labile} of 0.7 ± 0.1 at these stations indicates a relatively low contribution to $[Fe_{total}]$ from refractory material, consistent with elemental composition analyses of BNL particles that indicate a dominant hydrothermal source (Lee et al., this issue), and with the previously documented presence of Fe-rich sediments in the same region (Boström et al., 1969). This is further supported by $\delta^{56}Fe_{total}$ of BNL particles at Station 26 (-0.23 ‰ at 3900 m, -0.31 ‰ at 3960 m; Fig. 5b), which had f_{labile} of 0.8. These values are also close to plume $\delta^{56}Fe_{labile}$ and $\delta^{56}Fe_{total}$ values, consistent with the importance of plume-derived particles to local BNL pFe concentrations. Within the subset of western stations with BNLs, the heavier $\delta^{56}Fe_{labile}$ and lower f_{labile} values at Station 36 reflect the much

smaller hydrothermal signal in the overlying water column and the resulting heavier integrated water column $\delta^{56}Fe_{labile}$ at that station (Fig. 8a,d).

In the eastern part of the section, BNLs beneath the Peruvian Margin OMZ at Stations 1, 7 and 9 had relatively light $\delta^{56}Fe_{labile}$ values, averaging -0.72 ± 0.10 ‰ (n=11), with samples from the Station 1 BNL as light as -0.89 ‰ (Fig. 4). Similarly light $\delta^{56}Fe_{labile}$ values measured in BNL particles underneath the Mauritanian upwelling region during GA03 were attributed to the influence of isotopically light Fe(II) being released from sediment porewaters and precipitating upon interaction with oxic seawater (Revels et al., 2015a). Here, we propose that the light BNL $\delta^{56}Fe_{labile}$ is influenced by Fe oxyhydroxides that formed within the OMZ and settled through the water column. The BNL $\delta^{56}Fe_{labile}$ values for these stations are statistically indistinguishable to those measured within the OMZ, but distinct from those in the deep ocean at the same stations (Table 2). Although the near-seafloor formation of isotopically light Fe oxyhydroxides from porewater dFe(II) is a possibility, the lower flux of organic material to the deep ocean seafloor at these offshore stations reasons against a significant local reducing sedimentary source.

Significantly lower BNL f_{labile} values at these stations (0.3 ± 0.1) than in the overlying water column (Fig. 8b) are consistent with compositional analysis that suggests relatively high concentrations of lithogenic material within the nepheloid layers (Lam et al., this issue; Lee et al., this issue).

For eleven BNL samples collected at Stations 11, 13, 15 and 17, $\delta^{56}Fe_{labile}$ averaged -0.47 ± 0.07 ‰ − between values for BNLs nearer the Peruvian margin and those further west, and consistent with a mixture of hydrothermal and OMZ Fe oxyhydroxides contributing to [Fe_{labile}] at these stations. Though only two of these stations fell within the zonal extent of the OMZ at the time of sampling (Fig. 2), upper water column O_2 concentrations of below 50 μmol kg^{-1} extended as far west as Station 17. Similarly, although these stations lie to the east of the sampled hydrothermal plume, previous studies have also shown a hydrothermal influence in water column samples east of the SEPR (Fitzsimmons et al., 2016; Lonsdale, 1976).

The central BNL $\delta^{56}Fe_{labile}$ values were generally slightly (~0.1 ‰) lighter than those in the overlying water column (Fig. 8a), which may indicate temporal changes in

the extent of OMZ and hydrothermal influence on deep-sea pFe supply in the eastern Pacific. BNL f_{labile} at these stations (0.6 ± 0.2) more closely resembled that of the stations further west, due to the greater distance from the supply of lithogenic material near the Peruvian margin, and is consistent with elemental composition analyses that indicated enrichment in Fe relative to lithogenic Fe/Al ratios (Lee et al., this issue).

The relationship between depth-integrated water column and BNL $\delta^{56}Fe_{labile}$ values is shown in Fig. 8d. The two show a strong linear correlation (Pearson correlation coefficient, r=0.913, p<0.001), implying that BNL $\delta^{56}Fe_{labile}$ values are directly influenced by $\delta^{56}Fe_{labile}$ of the overlying water column. Assuming that BNL material is representative of surface sediments, this would mean that $\delta^{56}Fe_{labile}$ of surface sediments could be used as a tracer for the influence of prominent water column features such as hydrothermal plumes or oxygen minimum zones. This would only work in areas where sediments are oxic, so that the isotopic signature of the sedimented particles is not altered over time by processes such as dissimilatory iron reduction, but the findings presented here suggest that further investigation of this potential tracer would certainly be worthwhile in regions with low vertical flux of organic material.

5. Conclusions

Isotope measurements of "ligand-leachable" iron associated with 0.8–51 μm-sized particles from the US GEOTRACES GP16 section have highlighted important aspects of Fe biogeochemical cycling along the section, and the imprint they each leave on material reaching the sediment. A hydrothermal plume emanating from the SEPR was identified as a source of labile pFe to the deep ocean, as was the continental slope of the Peruvian margin, while export of labile pFe from the Peruvian shelf may be linked to redox cycling within the OMZ. Away from the shelf, upper ocean [Fe_{labile}] was very low, with variable $\delta^{56}Fe_{labile}$.

Particulate iron is composed primarily of labile Fe(III) oxyhydroxides in both the deep (2200–3000 m) hydrothermal plume that extends hundreds of kilometers westwards from the SEPR and within the OMZ that extends from the Peruvian continental shelf to ~100°W. But the isotopic signature of labile pFe within the OMZ ($\delta^{56}Fe_{labile} = -0.68 \pm$

0.32 ‰) is notably lighter than that within the hydrothermal plume ($\delta^{56}Fe_{labile} = -0.26 \pm$ 0.14 ‰). This most likely reflects the different isotopic signature of the source material from which the oxyhydroxides formed and/or isotope effects during formation. Within the hydrothermal plume, quantitative precipitation of a vent fluid with $\delta^{56}Fe \approx -0.2$ ‰ as it mixes with oxic seawater can explain the observed $\delta^{56}Fe_{labile}$ signal. In the OMZ, isotopically light dFe originally released from reducing shelf sediments undergoes seemingly non-oxygen dependent oxidation and precipitation, transferring the light isotopic signal from the dissolved to the labile particulate phase.

Beneath each of these features, BNL $\delta^{56}Fe_{labile}$ matches that of the elevated pFe concentrations in the water above. Labile pFe in nepheloid layers beneath the hydrothermal plume has $\delta^{56}Fe_{labile}$ of -0.34 ± 0.03 ‰ and constitutes the majority of the suspended pFe. Beneath the Peruvian Margin OMZ, nepheloid layer labile pFe makes a smaller contribution to the total, due to a greater supply of lithogenic material. At three stations with BNLs beneath the OMZ, nepheloid layer $\delta^{56}Fe_{labile}$ of -0.72 ± 0.10 ‰ mirrors that within the OMZ. At central stations, BNL $\delta^{56}Fe_{labile}$ reflects contributions of Fe oxyhydroxides from both the OMZ and hydrothermal processes. The similarity of $\delta^{56}Fe_{labile}$ values in BNLs to those of the overlaying hydrothermal or OMZ features suggests that, assuming that the nepheloid layer pFe is representative of that in surface sediments, $\delta^{56}Fe_{labile}$ of sediments could potentially be used to trace the past extent of hydrothermal plumes and OMZs through time.

6. Acknowledgements

References

Abadie, C., Lacan, F., Radic, A., Pradoux, C., Poitrasson, F., 2017. Iron isotopes reveal distinct dissolved iron sources and pathways in the intermediate versus deep Southern Ocean. Proc. Natl. Acad. Sci. 114, 858–863. doi:10.1073/pnas.1603107114

Beard, B.L., Johnson, C.M., Von Damm, K.L., Poulson, R.L., 2003. Iron isotope constraints on Fe cycling and mass balance in oxygenated Earth oceans. Geology 31, 629–632. doi:10.1130/0091-7613(2003)031<0629:IICOFC>2.0.CO;2

Bennett, S.A., Rouxel, O., Schmidt, K., Garbe-Schönberg, D., Statham, P.J., German, C.R., 2009. Iron isotope fractionation in a buoyant hydrothermal plume, 5°S Mid-Atlantic Ridge. Geochim. Cosmochim. Acta 73, 5619–5634. doi:10.1016/j.gca.2009.06.027

Berger, C.J.M., Lippiatt, S.M., Lawrence, M.G., Bru, 2008. Application of a chemical leach technique for estimating labile particulate aluminum, iron and manganese in the Columbia River plume and coastal waters off Oregon and Washington. J. Geophys. Res. Ocean. 113, C00B01. doi:10.1029/2007JC004703

Bishop, J.K.B., Lam, P.J., Wood, T.J., 2012. Getting good particles: Accurate sampling of particles by large volume in-situ filtration. Limnol. Oceanogr. Methods 10, 681–710. doi:10.4319/lom.2012.10.681

Boström, K., Peterson, M.N.A., Joensuu, O., Fisher, D.E., 1969. Aluminum-poor ferromanganoan sediments on active oceanic ridges. J. Geophys. Res. 74, 3261–3270. doi:10.1029/JB074i012p03261

Bowie, A.R., Maldonado, M.T., Frew, R.D., Croot, P.L., Achterberg, E.P., Mantoura, R.F.C., Worsfold, P.J., Law, C.S., Boyd, P.W., 2001. The fate of added iron during a mesoscale fertilisation experiment in the Southern Ocean. Deep. Res. Part II Top. Stud. Oceanogr. 48, 2703–2743. doi:10.1016/S0967-0645(01)00015-7

Boyd, P.W., Ellwood, M.J., 2010. The biogeochemical cycle of iron in the ocean. Nat. Geosci. 3, 675–682. doi:10.1038/NGEO964

Boyd, P.W., Ibisanmi, E., Sander, S.G., Hunter, K.A., Jackson, G.A., 2010. Remineralization of upper ocean particles: Implications for iron biogeochemistry.

Limnol. Oceanogr. 55, 1271–1288. doi:10.4319/lo.2010.55.3.1271

Burdige, D.J., 1993. The biogeochemistry of manganese and iron reduction in marine
sediments. Earth-Science Rev. 35, 249–284. doi:10.1016/0012-8252(93)90040-E

Chever, F., Rouxel, O.J., Croot, P.L., Ponzevera, E., Wuttig, K., Auro, M., 2015. Total
dissolvable and dissolved iron isotopes in the water column of the Peru upwelling
regime. Geochim. Cosmochim. Acta 162, 66–82. doi:10.1016/j.gca.2015.04.031

Conway, T.M., John, S.G., 2015. The cycling of iron, zinc and cadmium in the North
East Pacific Ocean - Insights from stable isotopes. Geochim. Cosmochim. Acta 164,
262–283. doi:10.1016/j.gca.2015.05.023

Conway, T.M., John, S.G., 2014. Quantification of dissolved iron sources to the North
Atlantic Ocean. Nature 511, 212–215. doi:10.1038/nature13482

Conway, T.M., Rosenberg, A.D., Adkins, J.F., John, S.G., 2013. A new method for
precise determination of iron, zinc and cadmium stable isotope ratios in seawater by
double-spike mass spectrometry. Anal. Chim. Acta 793, 44–52.
doi:10.1016/j.aca.2013.07.025

Cutter, G.A., Moffett, J.W., Nielsdóttir, M., Sanial, V., submitted. Multiple oxidation
state trace elements in low oxygen waters off Peru: in situ redox processes and
horizontal advective/diffusive transport. Mar. Chem.

Dauphas, N., Rouxel, O., 2006. Mass spectrometry and natural variations of iron
isotopes. Mass Spectrom. Rev. doi:10.1002/mas.20078

Dideriksen, K., Baker, J.A., Stipp, S.L.S., 2008. Equilibrium Fe isotope fractionation
between inorganic aqueous Fe(III) and the siderophore complex, Fe(III)-
desferrioxamine B. Earth Planet. Sci. Lett. 269, 280–290.
doi:10.1016/j.epsl.2008.02.022

Ellwood, M.J., Hutchins, D.A., Lohan, M.C., Milne, A., Nasemann, P., Nodder, S.D.,
Sander, S.G., Strzepek, R., Wilhelm, S.W., Boyd, P.W., 2015. Iron stable isotopes
track pelagic iron cycling during a subtropical phytoplankton bloom. Proc. Natl.
Acad. Sci. 112, E15–E20. doi:10.1073/pnas.1421576112

Fitzsimmons, J.N., Conway, T.M., Lee, J.-M., Kayser, R., Thyng, K.M., John, S.G.,
Boyle, E.A., 2016. Dissolved iron and iron isotopes in the southeastern Pacific
Ocean. Global Biogeochem. Cycles 30, 1372–1395. doi:10.1002/2015GB005357

Fitzsimmons, J.N., John, S.G., Marsay, C.M., Hoffman, C.L., Nicholas, S.L., Toner, B.M., German, C.R., Sherrell, R.M., 2017. Iron persistence in a distal hydrothermal plume supported by dissolved-particulate exchange. Nat. Geosci. 10, 195–201. doi:10.1038/NGEO2900

Frew, R.D., Hutchins, D.A., Nodder, S., Sanudo-Wilhelmy, S., Tovar-Sanchez, A., Leblanc, K., Hare, C.E., Boyd, P.W., 2006. Particulate iron dynamics during FeCycle in subantarctic waters southeast of New Zealand. Global Biogeochem. Cycles 20. doi:10.1029/2005GB002558

Fuenzalida, R., Schneider, W., Garcés-Vargas, J., Bravo, L., Lange, C., 2009. Vertical and horizontal extension of the oxygen minimum zone in the eastern South Pacific Ocean. Deep Sea Res. Part II Top. Stud. Oceanogr. 56, 992–1003. doi:10.1016/j.dsr2.2008.11.001

Heller, M.I., Lam, P.J., Moffett, J.W., 2016. Westward penetration of particulate and dissolved iron redox species from the Peruvian margin, in: Ocean Sciences Meeting, ASLO/AGU/TOS, New Orleans. p. CT23A-05.

Heller, M.I., Lam, P.J., Moffett, J.W., Till, C.P., Lee, J.-M., Toner, B.M., Marcus, M.A., 2017. Accumulation of Fe oxides in the Peruvian oxygen deficient zone implies non-oxygen dependent Fe oxidation. Geochim. Cosmochim. Acta 211, 174–193. doi:10.1016/j.gca.2017.05.019

Homoky, W.B., John, S.G., Conway, T.M., Mills, R. a, 2013. Distinct iron isotopic signatures and supply from marine sediment dissolution. Nat. Commun. 4, 2143. doi:10.1038/ncomms3143

Hong, H., Kester, D.R., 1986. Redox state of iron in the offshore waters of Peru. Limnol. Oceanogr. 31, 512–524. doi:10.4319/lo.1986.31.3.0512

Jenkins, W.J., Lott III, D.E., German, C.R., Cahill, K.L., Goudreau, J., Longworth, B., 2017. The deep distributions of helium isotopes, radiocarbon, and noble gases along the U.S. GEOTRACES East Pacific Zonal Transect (GP16). Mar. Chem. doi:10.1016/j.marchem.2017.03.009

Jickells, T.D., An, Z.S., Andersen, K.K., Baker, A.R., Bergametti, G., Brooks, N., Cao, J.J., Boyd, P.W., Duce, R.A., Hunter, K.A., Kawahata, H., Kubilay, N., LaRoche, J., Liss, P.S., Mahowald, N., Prospero, J.M., Ridgwell, A.J., Tegen, I., Torres, R., 2005.

Global iron connections between desert dust, ocean biogeochemistry, and climate. Science (80-.). 308, 67–71. doi:10.1126/science.1105959

John, S.G., Adkins, J., 2012. The vertical distribution of iron stable isotopes in the North Atlantic near Bermuda. Global Biogeochem. Cycles 26, 1–10. doi:10.1029/2011GB004043

John, S.G., Adkins, J.F., 2010. Analysis of dissolved iron isotopes in seawater. Mar. Chem. 119, 65–76. doi:10.1016/j.marchem.2010.01.001

John, S.G., Helgoe, J., Townsend, E., Weber, T., DeVries, T., Tagliabue, A., Moore, K., Lam, P., Marsay, C.M., Till, C., 2017. Biogeochemical cycling of Fe and Fe stable isotopes in the Eastern Tropical South Pacific. Mar. Chem. doi:10.1016/j.marchem.2017.06.003

John, S.G., Mendez, J., Moffett, J., Adkins, J., 2012. The flux of iron and iron isotopes from San Pedro Basin sediments. Geochim. Cosmochim. Acta 93, 14–29. doi:10.1016/j.gca.2012.06.003

Klar, J.K., James, R.H., Gibbs, D., Lough, A., Parkinson, I., Milton, J.A., Hawkes, J.A., Connelly, D.P., 2017. Isotopic signature of dissolved iron delivered to the Southern Ocean from hydrothermal vents in the East Scotia Sea. Geology 45, 351–354. doi:10.1130/G38432.1

Kondo, Y., Moffett, J.W., 2015. Iron redox cycling and subsurface offshore transport in the eastern tropical South Pacific oxygen minimum zone. Mar. Chem. 168, 95–103. doi:10.1016/j.marchem.2014.11.007

Kuss, J., Kremling, K., 1999. Spatial variability of particle associated trace elements in near-surface waters of the North Atlantic (30°N/60°W to 60°N/2°W), derived by large volume sampling. Mar. Chem. 68, 71–86. doi:10.1016/S0304-4203(99)00066-3

Labatut, M., Lacan, F., Pradoux, C., Chmeleff, J., Radic, A., Murray, J.W., Poitrasson, F., Johansen, A.M., Thil, F., 2014. Iron sources and dissolved-particulate interactions in the seawater of the Western Equatorial Pacific, iron isotope perspectives. Global Biogeochem. Cycles 28, 1044–1065. doi:10.1002/2014GB004928

Lacan, F., Radic, A., Jeandel, C., Poitrasson, F., Sarthou, G., Pradoux, C., Freydier, R., 2008. Measurement of the isotopic composition of dissolved iron in the open ocean.

Geophys. Res. Lett. 35. doi:10.1029/2008GL035841

Lam, P.J., Bishop, J.K.B., 2008. The continental margin is a key source of iron to the HNLC North Pacific Ocean. Geophys. Res. Lett. 35. doi:10.1029/2008GL033294

Lam, P.J., Bishop, J.K.B., Henning, C.C., Marcus, M.A., Waychunas, G.A., Fung, I.Y., 2006. Wintertime phytoplankton bloom in the subarctic Pacific supported by continental margin iron. Global Biogeochem. Cycles 20. doi:10.1029/2005GB002557

Lam, P.J., Lee, J.-M., Heller, M.I., Mehic, S., Xiang, Y., Bates, N., submitted. Size-fractionated distributions of suspended particle concentration and major phase composition from the U.S. GEOTRACES Eastern Pacific Zonal Transect (GP16). Mar. Chem.

Lee, J.-M., Heller, M.I., Lam, P.J., submitted. Size distribution of particulate trace elements in the U.S. GEOTRACES Eastern Pacific Zonal Transect (GP16). Mar. Chem.

Lonsdale, P., 1976. Abyssal circulation of the southeastern Pacific and some geological implications. J. Geophys. Res. 81, 1163. doi:10.1029/JC081i006p01163

Lupton, J.E., Craig, H., 1981. A major Helium-3 source at 15S on the East Pacific Rise. Science (80-.). 214, 13–18. doi:10.1126/science.214.4516.13

Mahowald, N.M., Baker, A.R., Bergametti, G., Brooks, N., Duce, R.A., Jickells, T.D., Kubilay, N., Prospero, J.M., Tegen, I., 2005. Atmospheric global dust cycle and iron inputs to the ocean. Global Biogeochem. Cycles. doi:10.1029/2004GB002402

Martin, J.H., Gordon, R.M., Fitzwater, S.E., 1991. The case for iron. Limnol. Oceanogr. 36, 1793–1802. doi:10.3389/fmicb.2011.00160

Millero, F.J., 1998. Solubility of Fe(III) in seawater. Earth Planet. Sci. Lett. 154, 323–329. doi:10.1016/S0012-821X(97)00179-9

Moffett, J.W., Goepfert, T.J., Naqvi, S.W.A., 2007. Reduced iron associated with secondary nitrite maxima in the Arabian Sea. Deep. Res. Part I Oceanogr. Res. Pap. 54, 1341–1349. doi:10.1016/j.dsr.2007.04.004

Moore, J.K., Braucher, O., 2008. Sedimentary and mineral dust sources of dissolved iron to the World Ocean. Biogeosciences 5, 631–656. doi:10.5194/bgd-4-1279-2007

Moore, J.K., Doney, S.C., Glover, D.M., Fung, I.Y., 2002. Iron cycling and nutrient-

limitation patterns in surface waters of the world ocean. Deep. Res. Part II Top. Stud. Oceanogr. 49, 463–507. doi:10.1016/S0967-0645(01)00109-6

Moore, J.K., Doney, S.C., Lindsay, K., 2004. Upper ocean ecosystem dynamics and iron cycling in a global three-dimensional model. Global Biogeochem. Cycles 18, 1–21. doi:10.1029/2004GB002220

Morel, F.M.M., Milligan, A.J., Saito, M.A., 2004. Marine bioinorganic chemistry: the role of trace metals in the oceanic cycles of major nutrients, in: Elderfield, H. (Ed.), Treatise on Geochemistry, Vol. 6: The Oceans and Marine Geochemistry. Elsevier-Pergamon, Oxford, pp. 113–143.

Noffke, A., Hensen, C., Sommer, S., Scholz, F., Bohlen, L., Mosch, T., Graco, M., Wallmann, K., 2012. Benthic iron and phosphorus fluxes across the Peruvian oxygen minimum zone. Limnol. Oceanogr. 57, 851–867. doi:10.4319/lo.2012.57.3.0851

Ohnemus, D.C., Auro, M.E., Sherrell, R.M., Lagerstrom, M., Morton, P.L., Twining, B.S., Rauschenberg, S., Lam, P.J., 2014. Laboratory intercomparison of marine particulate digestions including Piranha: a novel chemical method for dissolution of polyethersulfone filters. Limnol. Oceanogr. 12, 530–547. doi:10.4319/lom.2014.12.530

Ohnemus, D.C., Lam, P.J., 2015. Cycling of lithogenic marine particles in the US GEOTRACES North Atlantic transect. Deep. Res. Part II Top. Stud. Oceanogr. 116, 283–302. doi:10.1016/j.dsr2.2014.11.019

Radic, A., Lacan, F., Murray, J.W., 2011. Iron isotopes in the seawater of the equatorial Pacific Ocean: New constraints for the oceanic iron cycle. Earth Planet. Sci. Lett. 306, 1–10. doi:10.1016/j.epsl.2011.03.015

Resing, J.A., Sedwick, P.N., German, C.R., Jenkins, W.J., Moffett, J.W., Sohst, B.M., Tagliabue, A., 2015. Basin-scale transport of hydrothermal dissolved metals across the South Pacific Ocean. Nature 523, 200–203. doi:10.1038/nature14577

Revels, B.N., Ohnemus, D.C., Lam, P.J., Conway, T.M., John, S.G., 2015a. The isotopic signature and distribution of particulate iron in the North Atlantic Ocean. Deep. Res. Part II Top. Stud. Oceanogr. 116, 321–331. doi:10.1016/j.dsr2.2014.12.004

Revels, B.N., Zhang, R., Adkins, J.F., John, S.G., 2015b. Fractionation of iron isotopes

during leaching of natural particles by acidic and circumneutral leaches and development of an optimal leach for marine particulate iron isotopes. Geochim. Cosmochim. Acta 166, 92–104. doi:10.1016/j.gca.2015.05.034

Rouxel, O., Toner, B.M., Manganini, S.J., German, C.R., 2016. Geochemistry and iron isotope systematics of hydrothermal plume fall-out at East Pacific Rise 9°50'N. Chem. Geol. 441, 212–234. doi:10.1016/j.chemgeo.2016.08.027

Rudnicki, M.D., Elderfield, H., 1993. A chemical model of the buoyant and neutrally buoyant plume above the TAG vent field, 26 degrees N, Mid-Atlantic Ridge. Geochim. Cosmochim. Acta 57, 2939–2957. doi:10.1016/0016-7037(93)90285-5

Scholz, F., Hensen, C., Noffke, A., Rohde, A., Liebetrau, V., Wallmann, K., 2011. Early diagenesis of redox-sensitive trace metals in the Peru upwelling area - response to ENSO-related oxygen fluctuations in the water column. Geochim. Cosmochim. Acta 75, 7257–7276. doi:10.1016/j.gca.2011.08.007

Scholz, F., Löscher, C.R., Fiskal, A., Sommer, S., Hensen, C., Lomnitz, U., Wuttig, K., Göttlicher, J., Kossel, E., Steininger, R., Canfield, D.E., 2016. Nitrate-dependent iron oxidation limits iron transport in anoxic ocean regions. Earth Planet. Sci. Lett. 454, 272–281. doi:10.1016/j.epsl.2016.09.025

Scholz, F., Severmann, S., McManus, J., Hensen, C., 2014a. Beyond the Black Sea paradigm: The sedimentary fingerprint of an open-marine iron shuttle. Geochim. Cosmochim. Acta 127, 368–380. doi:10.1016/j.gca.2013.11.041

Scholz, F., Severmann, S., McManus, J., Noffke, A., Lomnitz, U., Hensen, C., 2014b. On the isotope composition of reactive iron in marine sediments: Redox-shuttle versus early diagenesis. Chem. Geol. 389, 48–59. doi:http://dx.doi.org/10.1016/j.chemgeo.2014.09.009

Severmann, S., Johnson, C.M., Beard, B.L., German, C.R., Edmonds, H.N., Chiba, H., Green, D.R.H., 2004. The effect of plume processes on the Fe isotope composition of hydrothermally derived Fe in the deep ocean as inferred from the Rainbow vent site, Mid-Atlantic Ridge, 36°14′N. Earth Planet. Sci. Lett. 225, 63–76. doi:10.1016/j.epsl.2004.06.001

Severmann, S., Johnson, C.M., Beard, B.L., McManus, J., 2006. The effect of early diagenesis on the Fe isotope compositions of porewaters and authigenic minerals in

continental margin sediments. Geochim. Cosmochim. Acta 70, 2006–2022. doi:10.1016/j.gca.2006.01.007

Severmann, S., McManus, J., Berelson, W.M., Hammond, D.E., 2010. The continental shelf benthic iron flux and its isotope composition. Geochim. Cosmochim. Acta 74, 3984–4004. doi:10.1016/j.gca.2010.04.022

Statham, P.J., German, C.R., Connelly, D.P., 2005. Iron (II) distribution and oxidation kinetics in hydrothermal plumes at the Kairei and Edmond vent sites, Indian Ocean. Earth Planet. Sci. Lett. 236, 588–896. doi:10.1016/j.epsl.2005.03.008

Staubwasser, M., Schoenberg, R., Von Blanckenburg, F., Krüger, S., Pohl, C., 2013. Isotope fractionation between dissolved and suspended particulate Fe in the oxic and anoxic water column of the Baltic Sea. Biogeosciences 10, 233–245. doi:10.5194/bg-10-233-2013

Staubwasser, M., von Blanckenburg, F., Schoenberg, R., 2006. Iron isotopes in the early marine diagenetic iron cycle. Geology 34, 629–632. doi:10.1130/G22647.1

Strzepek, R.F., Maldonado, M.T., Higgins, J.L., Hall, J., Safi, K., Wilhelm, S.W., Boyd, P.W., 2005. Spinning the "ferrous wheel": The importance of the microbial community in an iron budget during the FeCycle experiment. Global Biogeochem. Cycles 19. doi:10.1029/2005GB002490

Tovar-Sanchez, A., Sanudo-Wilhelmy, S.A., Garcia-Vargas, M., Weaver, R.S., Popels, L.C., Hutchins, D.A., 2003. A trace metal clean reagent to remove surface-bound iron from marine phytoplankton. Mar. Chem. 82, 91–99. doi:10.1016/S0304-4203(03)00054-9

Vedamati, J., Goepfert, T., Moffett, J.W., 2014. Iron speciation in the eastern tropical South Pacific oxygen minimum zone off Peru. Limnol. Oceanogr. 59, 1945–1957. doi:10.4319/lo.2014.59.6.1945

Fig. 1: Map of the US GEOTRACES GP16 East Pacific Zonal Transect, showing stations where in situ pumps were deployed.

Fig. 2: Distribution and characterization of pFe from the GP16 transect: (*a*) labile (ligand-leachable) pFe concentrations, [Fe$_{labile}$]; (*b*) total pFe concentrations, [Fe$_{total}$]; (*c*) labile pFe stable iron isotope ratios, δ^{56}Fe$_{labile}$; (*d*) fractional contribution of labile pFe to total pFe, *f$_{labile}$*. Lower panels show the full depth profiles while upper panels show expanded profiles of the upper 1000 m. Dotted outline in top panels indicates extent of the oxygen minimum zone (O$_2$ <20 μmol kg^{-1}). Dashed line in bottom panels indicates the 75 fmol kg^{-1} contour of ^{3}He$_{xs}$, relating to a neutrally buoyant hydrothermal plume spreading west from Station 18.

Fig. 3: Depth profiles of labile pFe concentration by station. Note different depth scales for Stations 2–5, and varying concentration scales in the different plots.

Fig. 4: Depth profiles of the iron stable isotope signature (δ^{56}Fe) of labile pFe by station. Note different depth scales for Stations 2–5 and different δ^{56}Fe scale for Stations 25 and 26.

Fig. 5: Concentration and isotope ratio data for labile and total pFe at Stations 26 and 36. (*a*) [Fe$_{labile}$] and [Fe$_{total}$] at Station 26. (*b*) δ^{56}Fe$_{labile}$ and δ^{56}Fe$_{total}$ at Station 26. (*c*) [Fe$_{labile}$] and [Fe$_{total}$] at Station 36. (*d*) δ^{56}Fe$_{labile}$ and δ^{56}Fe$_{total}$ at Station 36.

Fig. 6: Comparison of [Fe$_{labile}$] and [Fe$_{total}$] for different subsets of the section data. Main panel shows distribution of concentrations for 0–5 nM samples. Inset panel includes high concentration samples, with extent of the main panel indicated by the red box. Ranges and medians of [Fe$_{labile}$] and of *f$_{labile}$* for each subset of data are given in Table 2.

Fig. 7: Comparison of labile pFe and dFe distributions. (*a*) [Fe$_{labile}$] data (dots) overlaid on dFe concentration data. Contours are for 1 nM (dashed) and 0.1 nM (solid) dFe. (*b*) δ^{56}Fe$_{labile}$ data (dots) overlaid on δ^{56}Fe$_{diss}$ data. Contour is for δ^{56}Fe$_{diss}$ of 0 ‰.

Fig. 8: Comparison of [Fe_{labile}]-weighted, depth-integrated $\delta^{56}Fe_{labile}$ and f_{labile} for water column and BNL samples, by station. (**a**) change in water column and BNL $\delta^{56}Fe_{labile}$ as a function of location, (**b**) change in water column and BNL f_{labile} as a function of location, (**c**) comparison of water column, hydrothermal plume and BNL depth-integrated $\delta^{56}Fe_{labile}$ at Stations 25–30, (**d**) the relationship between water column and BNL $\delta^{56}Fe_{labile}$.
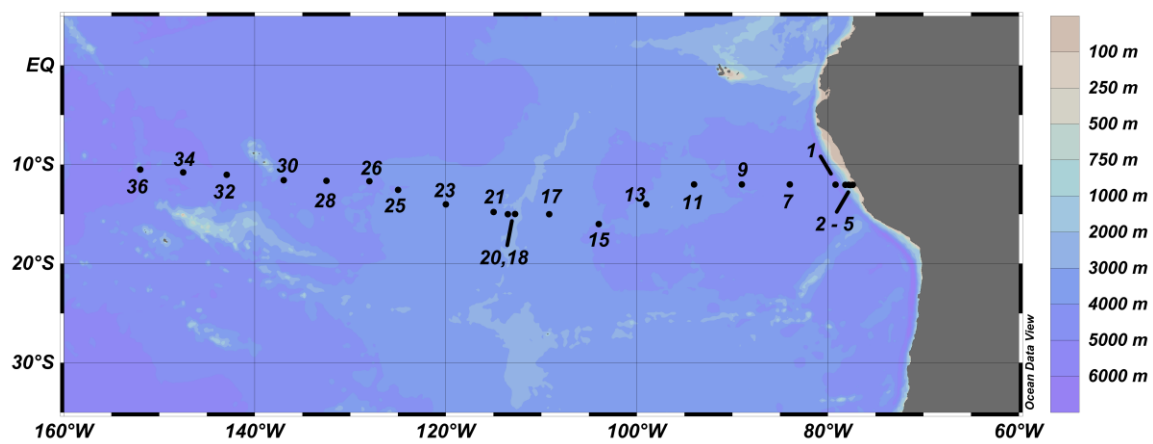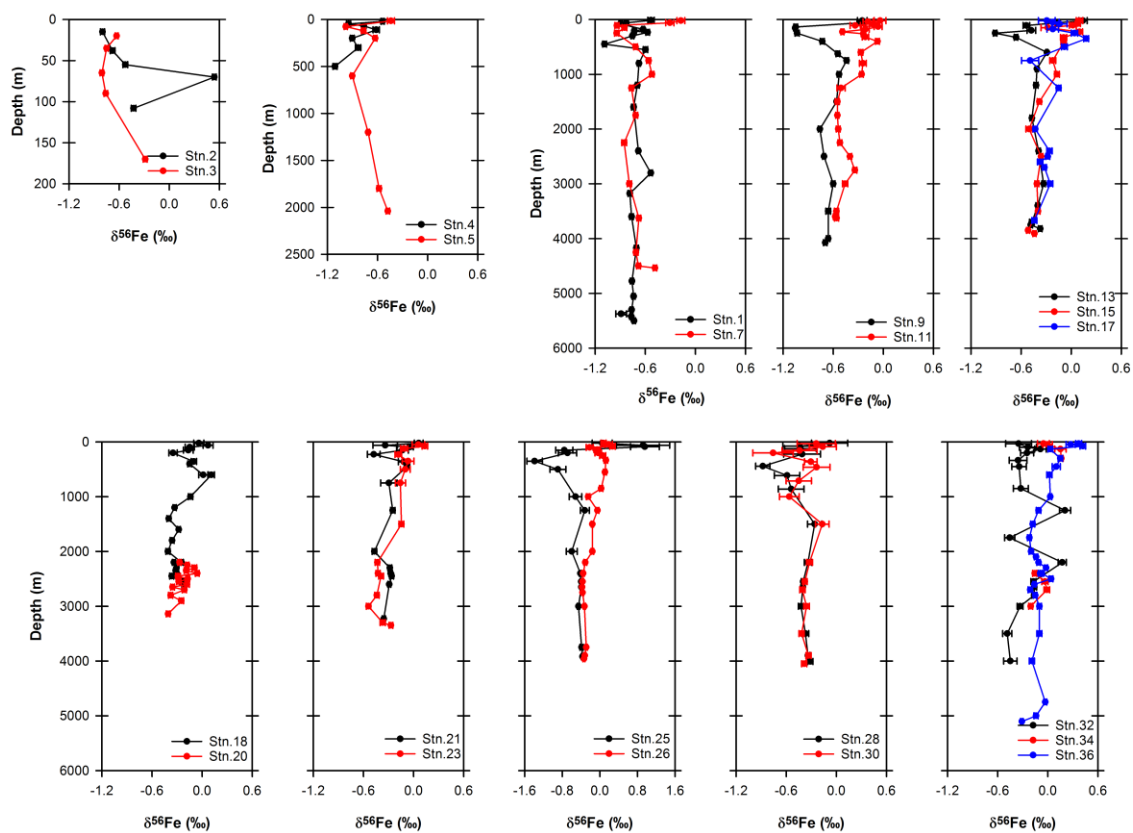
Figure 1
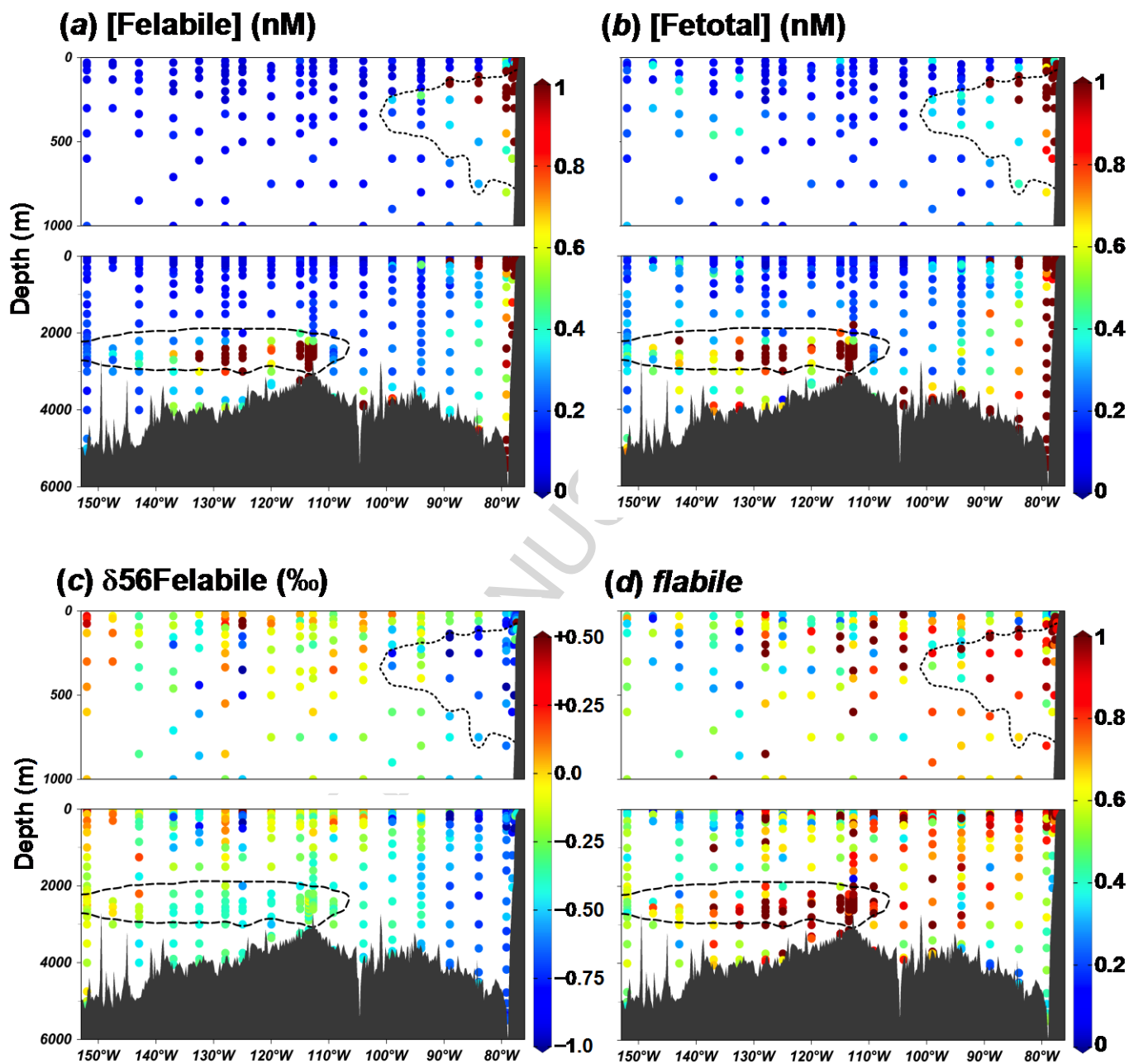
Figure 2
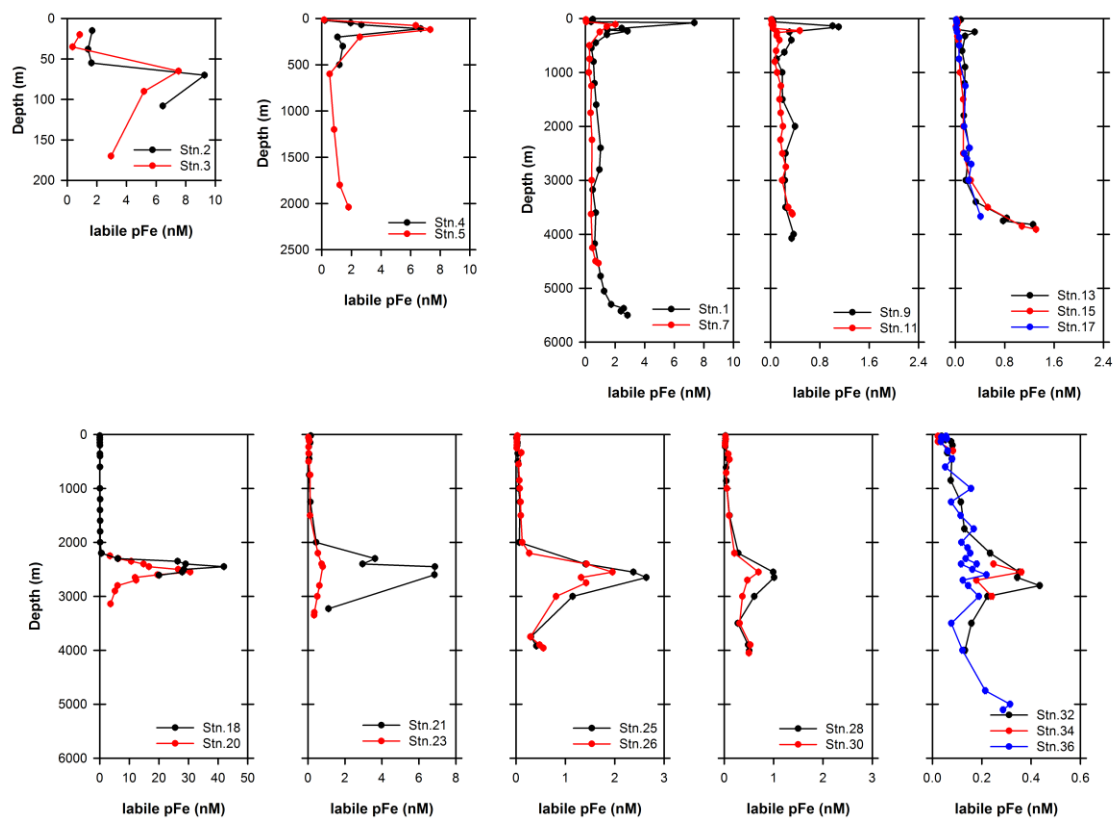
Figure 3

Figure 4

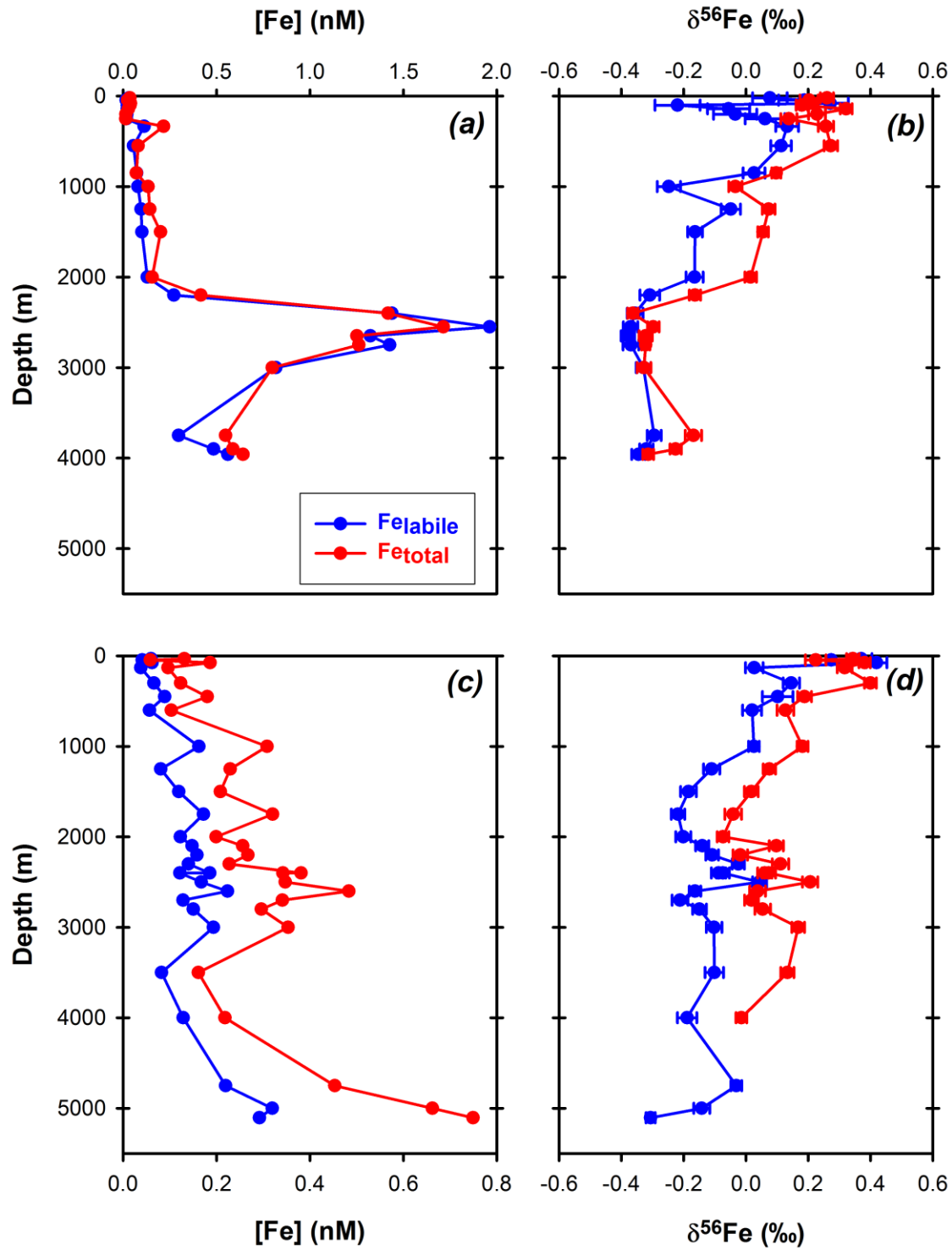Figure 5

Figure 6

(a) **Fe concentration (nM)**

(b) **δ56Fe (‰)**
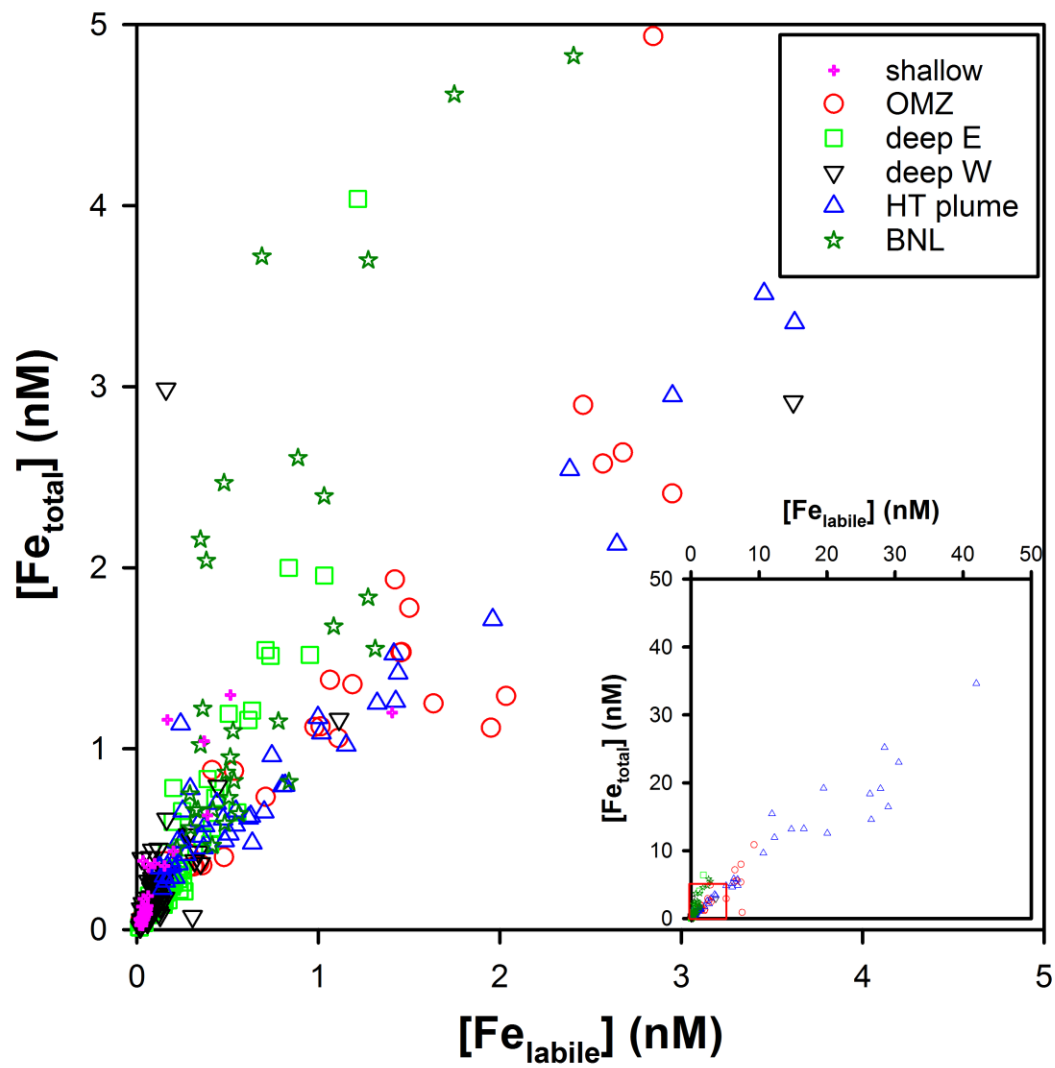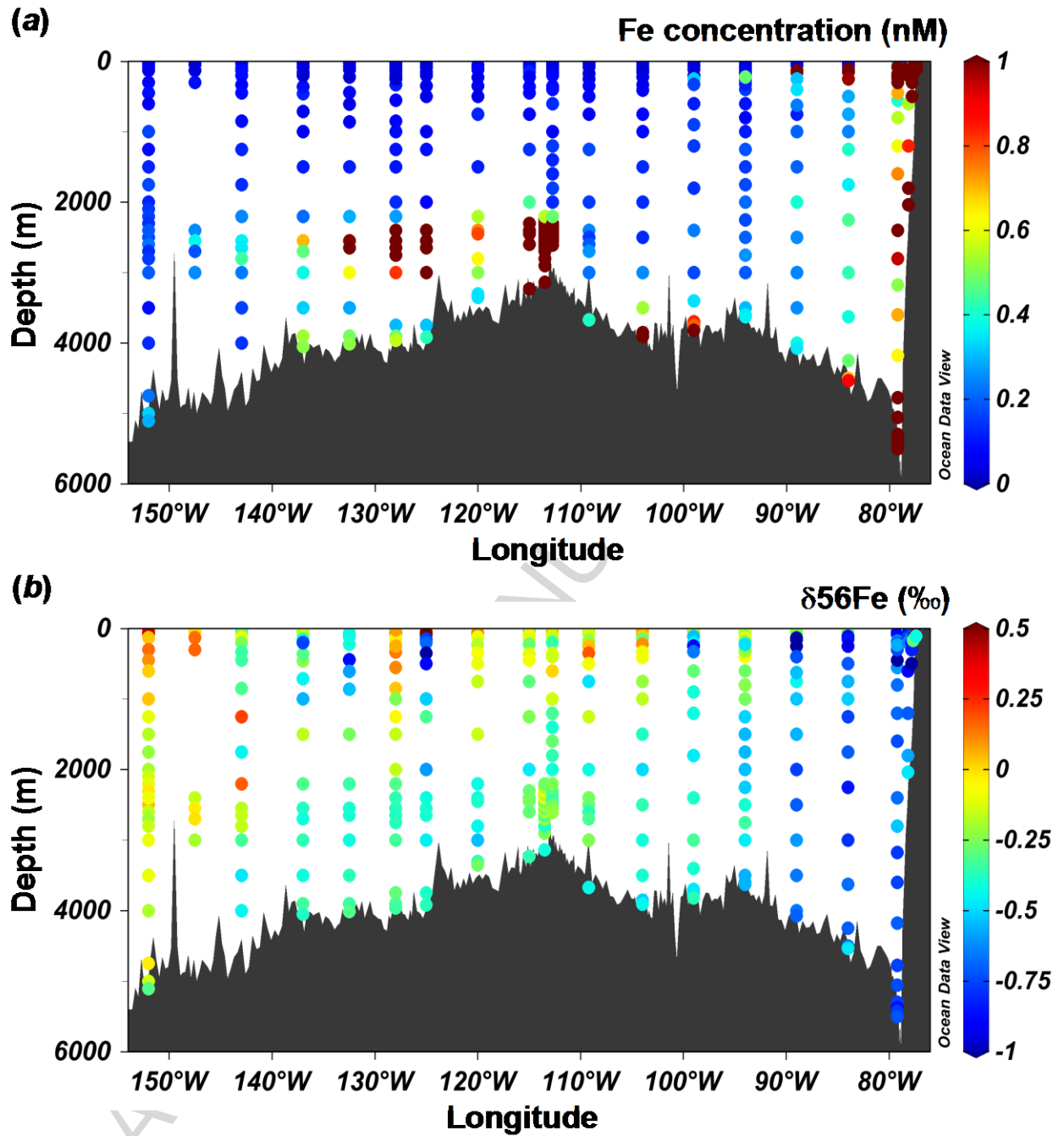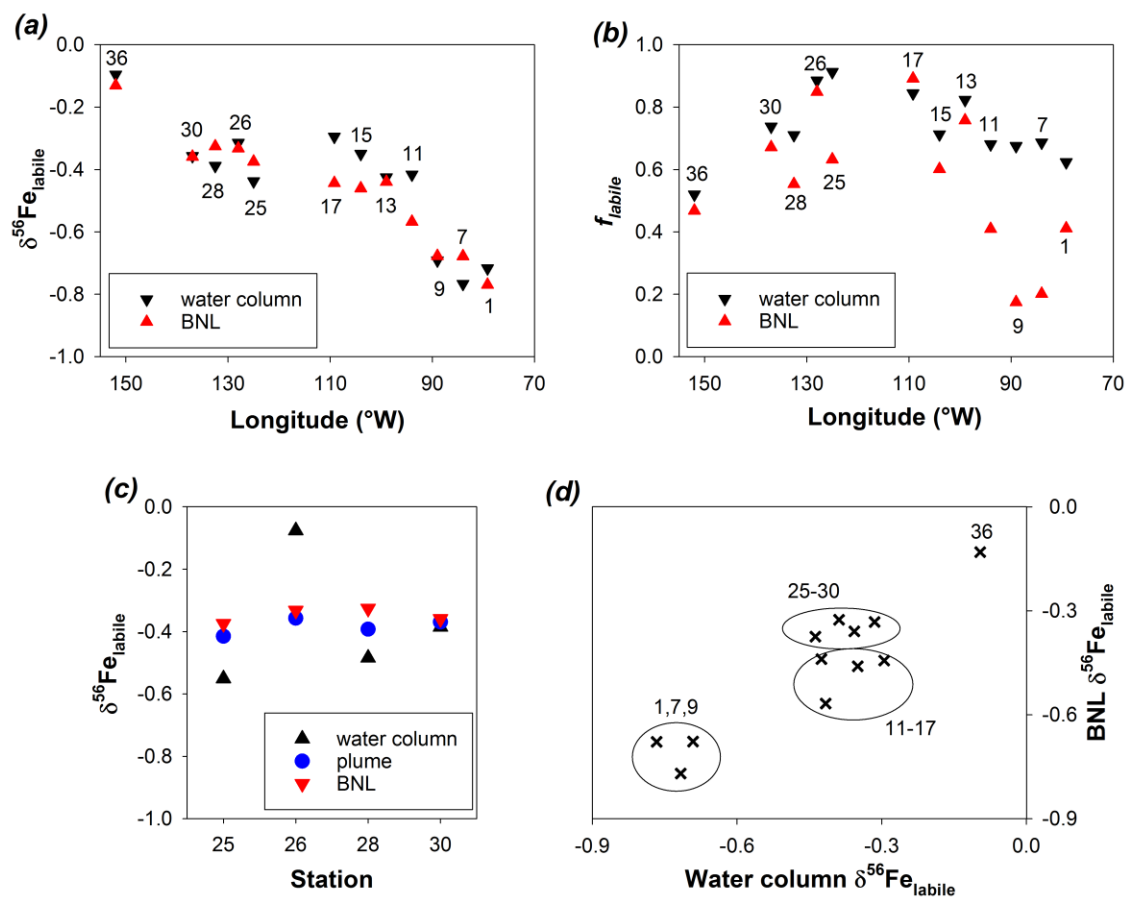

Figure 7

Figure 8

Table 1: Summary of blanks and detection limits associated with oxalate-EDTA leach treatment. Samples were corrected for a leach blank and dipped filter blank. Detection limits relate to total blank corrections.

	Leach Fe blank (ng g^{-1})	Dipped filter Fe blank (ng g^{-1})	Detection limit from combined blank (ng g^{-1})	Median blank contribution to sample Fe	No. of samples
Batch 1	13.3 ± 0.2 (*n*=4)	7.5 ± 4.4 (*n*=34)	13.1	5 %	247
Batch 2	122.4 ± 0.8 (*n*=4)	7.5 ± 4.4 (*n*=34)	13.3	48 %	94

Table 2: Regional and depth-related differences in [Fe$_{labile}$], δ^{56}Fe$_{labile}$ and f_{labile} along the GP16 section. OMZ = oxygen minimum zone, HT plume = hydrothermal plume, BNL = benthic nepheloid layers.

	[Fe$_{labile}$] (nM)		δ^{56}Fe$_{labile}$ (‰)			f_{labile}		n
	range	median	range	mean ±	median	range	median	
Surface	0.02–	0.04	–0.83–	–0.26 ±	–0.22	0.1–1	0.6	19
Surface	0.01–	0.03	–0.44–	+0.06 ±	+0.02	0.1–	0.5	26
OMZ	0.02–	1.2	–1.11–	–0.68 ±	–0.75	0.3–1	0.9	41
Deep ocean	0.01–	0.19	–0.85–	–0.44 ±	–0.46	0.3–1	0.7	65
Deep ocean	0.02–	0.08	–1.39–	–0.26 ±	–0.25	0.1–1	0.5	86
HT plume	0.12–	0.82	–0.54–	–0.26 ±	–0.28	0.2–1	1	67
BNL	0.22–	0.52	–0.89–-	–0.50 ±	–0.48	0.2–1	0.5	32